NASA TECHNICAL NOTE

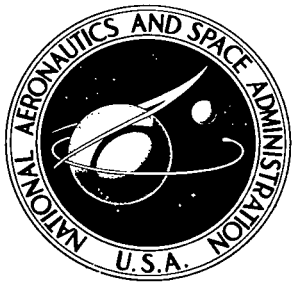

NASA TN D-6789

JET EFFECTS ON THE DRAG OF CONICAL AFTERBODIES AT SUPERSONIC SPEEDS

by William B. Compton III

Langley Research Center
Hampton, Va. 23365

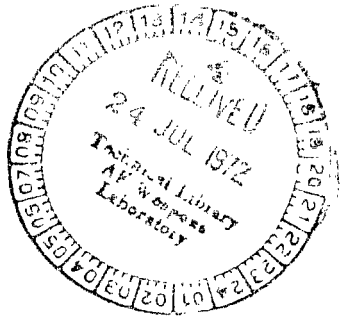

NATIONAL AERONAUTICS AND SPACE ADMINISTRATION • WASHINGTON, D. C. • JULY 1972

1. Report No.	2. Government Accession No.	3. Recipient's Catalog No.
NASA TN D-6789		

4. Title and Subtitle	5. Report Date
JET EFFECTS ON THE DRAG OF CONICAL AFTERBODIES AT SUPERSONIC SPEEDS	July 1972
	6. Performing Organization Code

7. Author(s)	8. Performing Organization Report No.
William B. Compton III	L-8139
	10. Work Unit No.
9. Performing Organization Name and Address	764-74-02-02
NASA Langley Research Center Hampton, Va. 23365	11. Contract or Grant No.
	13. Type of Report and Period Covered
12. Sponsoring Agency Name and Address	Technical Note
National Aeronautics and Space Administration Washington, D.C. 20546	14. Sponsoring Agency Code

15. Supplementary Notes

16. Abstract

A parametric investigation has been conducted to determine the jet effects on the boattail drag of nozzles with truncated conical afterbodies. The boattail drag for nozzle configurations with boattail angles of 3^{o}, 5^{o}, and 10^{o} and ratios of boattail length to maximum diameter of 1.0, 0.8, and 0.6 was compared for the jet-off condition and for a wide range of jet pressure ratios. A nozzle configuration with a circular-arc boattail was tested also. The tests were run at Mach numbers of 1.83 and 2.20 with the model at an angle of attack of 0^{o}.

17. Key Words (Suggested by Author(s))	18. Distribution Statement
Jet interference Boattail drag Conical afterbodies Convergent-divergent nozzles Supersonic speeds	Unclassified – Unlimited

19. Security Classif. (of this report)	20. Security Classif. (of this page)	21. No. of Pages	22. Price*
Unclassified	Unclassified	49	$3.00

*For sale by the National Technical Information Service, Springfield, Virginia 22151

JET EFFECTS ON THE DRAG OF CONICAL AFTERBODIES AT SUPERSONIC SPEEDS

By William B. Compton III
Langley Research Center

SUMMARY

A parametric investigation has been conducted in the Langley 4- by 4-foot supersonic pressure tunnel to determine the jet effects on the boattail drag of nozzles with truncated conical afterbodies. The boattail drag for nozzle configurations with boattail angles of 3^{o}, 5^{o}, and 10^{o} and ratios of boattail length to maximum diameter of 1.0, 0.8, and 0.6 was compared for the jet-off condition and for a wide range of jet pressure ratios. The different nozzle configurations represented various supersonic positions of each of three variable-flap convergent-divergent nozzles of different lengths. A nozzle configuration with a circular-arc boattail was tested also. The tests were run at Mach numbers of 1.83 and 2.20 with the model at an angle of attack of 0^{o}. The Reynolds number per meter was 14.70×10^{6} and 12.20×10^{6} at the Mach numbers of 1.83 and 2.20, respectively.

Results indicate that for these Mach numbers, at jet-exit static-pressure ratios below about 2.5 the effect of the jet is generally confined to a small area at the rear of the boattail. Also, there are indications that the jet-exit static-pressure ratio must be well above 1 before the trailing-edge pressure is affected by the jet. The jet exhaust generally had a greater influence on both the boattail pressures and the drag at a Mach number of 1.83 than at 2.20. The exhaust jet had very little interference effect on the boattail drag of the configurations with boattail angles of 3^{o} and 5^{o}; however, the interference effect was more pronounced for the configurations with a boattail angle of 10^{o}. Shortening the boattail always reduced boattail drag for a given boattail angle and static-pressure ratio.

INTRODUCTION

Aircraft which have operational capabilities at subsonic, transonic, and supersonic speeds require variable-geometry exhaust nozzles for which both the internal expansion ratio and the external boattail angle must change with Mach number and altitude for optimum performance. The wide ranges of boattail angles and external geometric variations that are possible with engines proposed for these multimission aircraft, together with the exhaust from their nozzles, have made precise prediction of the nozzle boattail drag diffi-

cult. Consequently, at the present time, experimental methods are generally used to obtain accurate nozzle drag and jet interference.

The jet interference effects on the boattail pressures can be large, particularly at subsonic speeds, for nozzles with large boattail angles and with the jet operating underexpanded. The present investigation, which was conducted in the Langley 4- by 4-foot supersonic pressure tunnel to provide parametric information on jet interference for the variable-flap type of convergent-divergent nozzle, extended the Mach number range of an investigation conducted in the Langley 16-foot transonic tunnel (ref. 1). Reference 1 gives an extensive list of other investigations of jet interference on boattail drag. In the present investigation, a nacelle model which supplied air for the jet exhaust was used to test a series of fixed conical-boattail convergent-divergent nozzles. The geometric variables were conical-boattail angle, nozzle length, and exit area. Data were obtained over a wide range of jet pressure ratios at free-stream Mach numbers of 1.83 and 2.20, at an angle of attack of 0^{o}. For the Mach numbers and the nozzle expansion ratios of the configurations of this investigation, the jet interference effects on the boattail drag should be similar to those for air-breathing turbine engines. Information on a reference nozzle with a circular-arc boattail is included in the appendix.

SYMBOLS

A	area, meters^2
A_m	maximum cross-sectional area of model, meters^2
$C_{D,\beta}$	boattail pressure-drag coefficient, $\frac{D_\beta}{qA_m}$
$C_{p,\beta}$	boattail pressure coefficient, $\frac{p_\beta - p_\infty}{q}$
c	length of convergent section of nozzle (see fig. 4), meters
D_β	boattail pressure drag, newtons
d	diameter, meters
f	axial distance from nozzle throat, positive aft (see fig. 4), meters
L	boattail length measured in axial direction (see fig. 4), meters
l	length of boattail flap measured parallel to boattail surface (see fig. 4), meters

M	free-stream Mach number
p	pressure, newtons/meter^2
q	free-stream dynamic pressure, newtons/meter^2
s	distance from nozzle throat to exit (see fig. 4), meters
x	axial distance from boattail corner, positive aft (see fig. 4), meters
α	nozzle divergence half-angle (see fig. 4), degrees
β	boattail angle, angle between axis of symmetry and generatrix of model afterbody (see fig. 4), degrees
$\Delta C_{p,\beta_e}$	difference between boattail trailing-edge pressure coefficients at jet-on and jet-off conditions
δ	calculated initial plume inclination angle, $\alpha + \Delta\nu$, degrees
ϵ_e	nozzle internal-expansion ratio, A_e/A_{th}
$\zeta = \delta + \beta$	
θ	nozzle convergence half-angle (see fig. 4), degrees
ν_1	Prandtl-Meyer angle required to expand jet flow to jet exit conditions, degrees
ν_2	Prandtl-Meyer angle required to expand jet flow to conditions just downstream of jet exit, degrees
$\Delta\nu$	difference between ν_2 and ν_1, degrees
ϕ	angular location measured in a plane perpendicular to axis of symmetry of model, clockwise direction positive when viewed from rear, 0^o at top of model (see fig. 4), degrees

Subscripts:

b	base

des	design
e	exit
j	jet
m	maximum
t	total
th	throat
β	boattail
∞	free stream

APPARATUS AND PROCEDURE

Wind Tunnel

The investigation was conducted in the Langley 4- by 4-foot supersonic pressure tunnel, which is a single-return, continuous-flow tunnel capable of operating at stagnation pressures of 28 to 207 kN/m^2 at a stagnation temperature of approximately 316 K. By use of interchangeable nozzle blocks, the Mach number can be varied from 1.41 to 2.20.

Model

The basic model to which nozzle configurations were attached was a cone-cylinder nacelle with a rounded shoulder at the junction of the nose and the cylindrical section. (See fig. 1.) A continuous flow of dry, high-pressure air at a total temperature of approximately 270 to 300 K was used for the jet exhaust. Boundary-layer transition was fixed at 2.54 centimeters from the nose of the model by a strip of No. 80 carborundum grit approximately 5 millimeters wide. The model was supported from the tunnel sidewall by a 5-percent-thick strut swept back with respect to the model and having a leading-edge sweep of 45^o. Figure 2 shows the area distributions for the model with a 5^o boattail angle and for the support strut. The details of the model, including the air introduction arrangement, are shown in figure 3, with the path of the air indicated by arrows.

The configurations investigated were part of a series simulating various positions of each of three variable-flap convergent-divergent nozzles. The series was formulated by assuming that a variable-geometry convergent-divergent nozzle with a ratio of flap length to maximum diameter of 1.0 would have a 0^o boattail angle at a design jet total-

pressure ratio of 34. The external geometry of the configurations was varied only aft of axial station 104.14, the location of the theoretical hinge point for the nozzle flaps. The fixed boattail angles β selected for investigation at supersonic speeds were 3^{o}, 5^{o}, and 10^{o} for each of the three nozzles, which had respective ratios of flap length to maximum diameter of 1.0, 0.8, and 0.6. The original design philosophy of having three nozzles of different lengths was to investigate the trade-off between boattail drag and internal performance as the nozzle was shortened. Reference 1 gives further details.

A sketch of a typical variable-flap nozzle configuration is presented in figure 4, and pertinent geometric parameters are listed for all configurations in the series. Those not tested in this investigation are indicated by asterisks. At the theoretical hinge point of the nozzle flaps, all nozzles had a cross-sectional area of 182.4 cm^2. The junction of the cylindrical section and the boattail was machined as a sharp corner and was at the same station for all the variable-flap nozzle configurations. In keeping with the variable-flap design, the difference between the exit and base diameters was kept small. (See fig. 4.) A more extensive discussion of the basic model and the nozzle configuration series is given in reference 1.

Instrumentation and Tests

Static pressures on the boattail surface, in the divergent part of the nozzles, on the cylindrical portion of the model, and in the model-shell gap were measured with strain-gage pressure transducers mounted in pressure scanning valves remotely located from the model. The locations of the static-pressure orifices are given in tables I and II. The total temperature and pressure of the jet flow ahead of the nozzle throat were measured with a single thermocouple probe and a single total-pressure probe. The measurement of average total pressure with only one probe was found to be acceptable by making pretest rake surveys for several nozzles with various throat diameters. These surveys indicated that the total-pressure profile in this region was essentially flat for all sizes of nozzles used in this investigation. All total-pressure measurements were made with individual pressure transducers.

The tests were conducted at Mach numbers of 1.83 and 2.20 with the model at an angle of attack of 0^{o}. A sweep of the desired jet pressure-ratio range was made in discrete steps from the lowest ratio to the maximum, and repeat points were taken as the pressure ratio was lowered. A jet-off point was taken at the beginning and end of every sweep. The jet pressure ratio was held constant as each point of data was taken.

The dewpoint of the tunnel was held at 244 K or less to avoid condensation. The investigation was conducted at a total pressure of 124.12 kN/m^2 which, with a total temperature of approximately 316 K, gave Reynolds numbers per meter of 14.70×10^6 and 12.20×10^6 at the Mach numbers of 1.83 and 2.20, respectively.

Data Reduction

The boattail drag coefficient $C_{D,\beta}$ presented in this paper is the coefficient of the nozzle external pressure drag on the axially projected area from A_m to A_b. No attempt was made to include the forces on the small rim at the nozzle exit between d_b and d_e. (See fig. 4.) The boattail drag coefficient is based on the maximum cross-sectional area of the model and was computed by assigning an incremental area (projected on a plane normal to the axis of symmetry) to each pressure orifice at $\phi = 0^o$ and using the equation

$$C_{D,\beta} = \frac{1}{qA_m} \sum_{i=1}^{n} (p_\infty - p_i) A_{\beta,i}$$

To compare the effect of the jet plume on the boattail pressures of the different configurations, an initial inclination angle of the jet plume was calculated for conditions at which the nozzle was flowing full and at which there was a large pressure rise at the trailing edge of the boattail. It was assumed that under these conditions the flow at this point would be separated or the boundary-layer thickness would be increased. Hence, the trailing-edge shock would be moved up the boattail, and the pressure at the trailing edge of the boattail would be very nearly that to which the jet exhaust was initially expanding on leaving the nozzle. These assumptions, together with the measured boattail static pressure nearest the trailing edge p_{β_e}, were used to obtain the static pressure in the jet exhaust immediately behind the boattail trailing edge. This pressure, the measured static pressure at the nozzle exit p_e, and the jet total pressure were used to compute the turning angles ν_2 and ν_1 for the jet flow from the formulas given in reference 2. The location of these pressures and the geometric angles used in the following calculations are illustrated in sketch (a).

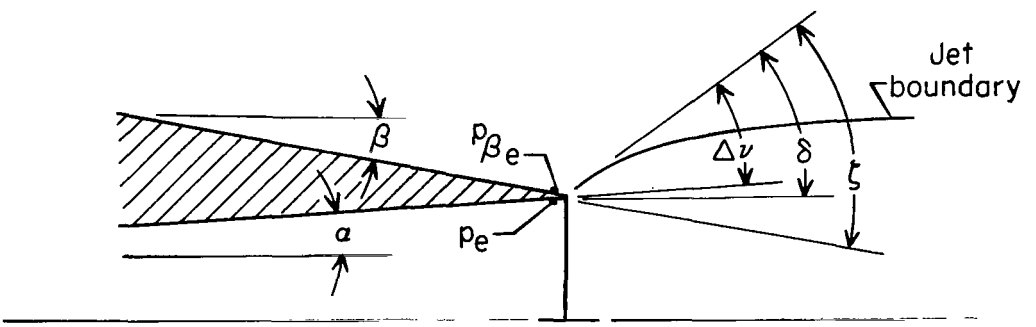

Sketch (a)

The initial turning angle of the jet on leaving the nozzle is then

$$\Delta\nu = \nu_2 - \nu_1$$

and the calculated initial plume inclination angle is

$$\delta = \alpha + \Delta\nu$$

where α is the nozzle divergence half-angle.

If the external flow on the boattail had not separated, or if the boundary layer had not thickened, the external flow would have to turn through an angle of

$$\zeta = \beta + \delta$$

at the boattail trailing edge. This angle was used to try to correlate the effect of the jet plume on the boattail pressures for the different nozzles.

RESULTS AND DISCUSSION

Because the boundary-layer thickness and the flow field in general can affect boattail drag, a brief description of the flow field about the model is included. A flow-field survey was conducted at a Mach number of 2.20 for the model with a cylindrical afterbody attached, and the results of the survey are reported in reference 3. Results indicated that the strut had very little effect on the surface pressure distribution of a cylindrical afterbody. The measured surface pressures on the model afterbody agreed very well with those predicted by the method of characteristics. Boundary-layer total-pressure profiles, which were measured at model stations of 104.14 and 110.29 centimeters, showed that the boundary-layer thickness was approximately 0.1 of the model diameter and was generally the same at all meridians except behind the strut, where there was a large loss in total pressure. Reynolds number variation from 1.55×10^6 to 2.07×10^6, based on body diameter, had only small effects on the boundary-layer profiles. The same results would be expected at a Mach number of 1.83. Further information on the flow field is presented in reference 3.

Figure 5 presents the pressure distributions at various meridians on an afterbody with $\beta = 10^\circ$ and $l/d_m = 1.0$. There is only a slight difference between the pressure coefficients of the top and bottom rows; however, only the pressures on the top row were used for purposes of comparison and integration into drag.

In figure 6 the measured boattail pressure distributions of the configurations with $l/d_m = 1.0$ are compared with distributions calculated by the method of characteristics,

assuming free-stream conditions ahead of the boattail. The comparisons are for the jet-off case. Agreement between the measured and theoretical values of the pressure coefficients is, in general, excellent. The agreement at the boattail trailing edge as well as farther forward indicates that at Mach numbers of 1.83 and 2.20 the boattail trailing-edge pressure is not affected by the base pressure for $l/d_m = 1.0$ and $\beta = 3^o$, 5^o, and 10^o.

Figure 7 presents boattail pressure distributions at several values of jet pressure ratio for each of the nozzles tested. Both the total-pressure and static-pressure ratios at each condition are indicated on the plots. The divergence half-angle α for each nozzle is shown also. Instead of jet total-pressure ratio, most of the comparisons are made on the basis of jet static-pressure ratio, a parameter more closely associated with jet interference.

At the Mach numbers of 1.83 and 2.20, below static-pressure ratios of 2.5 the effect of the jet on the boattail pressures is mostly confined to a small region at the rear of the nozzle. This is contrary to results for subsonic flow, where the jet effects may extend over the entire boattail length, an effect shown in the top part of figure 8 (from ref. 1). Inspection of figure 7 and the bottom part of figure 8 reveals that for a given configuration and jet pressure ratio, for the supersonic Mach numbers shown, the lower the Mach number, the more the jet affects the boattail trailing-edge pressures. It also appears that for a specific pressure ratio, the lower the supersonic Mach number, the farther forward the jet effects extend. However, an accurate determination of the extent of the region affected by the jet is precluded by the boattail orifice spacing. The pressure distributions for the 3^o and 5^o boattails indicate that the exit static-pressure ratio must be well above 1 before the trailing-edge pressure is affected by the jet. Also, for a particular configuration, the pressure ratio at which the trailing-edge pressure starts to rise increases with Mach number.

To determine the relative jet effects on the boattail pressures for different boattail angles and lengths, it is desirable to compare different nozzles at the same conditions of the jet exhaust. However, the various nozzle expansion ratios and divergence angles of the nozzles tested precluded such a direct comparison. It was believed that for these boattails and supersonic Mach numbers, plume blockage would generally create most of the jet effects. Therefore, to compare the jet effects of the different boattails, an initial inclination angle of the jet plume with the jet axis was calculated for each nozzle at several jet pressure ratios. This angle δ was then used as a parameter in comparing the jet interference on the boattail pressures of the various configurations. To understand the assumptions made in calculating δ, consider figure 9, a shadowgraph of a 10^o boattailed nozzle at a high jet pressure ratio and a corresponding sketch of the flow at the boattail. When the jet plume causes the shock at the nozzle exit to detach and move up the boattail, the boundary layer downstream of the first leg of the shock has either thickened or separated. It was assumed that under these conditions no shocks would

extend to the downstream end of the boattail surface, so p_{β_e}, the boattail pressure at this point, would be the pressure to which the jet was initially expanding. Then the measured value of this pressure and the measured value of p_e, the internal pressure nearest the nozzle exit, were used to calculate the initial inclination angle of the jet by the method described in the section "Data Reduction." The calculations were made only for points for which the boattail trailing-edge pressure coefficient was substantially higher than the jet-off value. The large rise indicated that the trailing-edge shock had moved upstream on the boattail. Under these conditions, the nozzle flow was also underexpanded.

Figure 10 shows the effect of δ on $\Delta C_{p,\beta_e}$, the change in the boattail trailing-edge pressure coefficient from the jet-off value, for the various boattail configurations tested. The figure indicates that, as would be expected, for a particular configuration the pressure rise caused by a given plume angle is greater at a Mach number of 1.83 than at 2.20.

In figure 11, $\Delta C_{p,\beta_e}$ is shown as a function of ζ, the hypothetical total angle through which the flow on the boattail would have to turn at the trailing edge. The plot was made in an attempt to correlate the effect of the jet plume on $\Delta C_{p,\beta_e}$ for the different boattail angles. Since the points for the various boattail angles do not fall on the same curve, the figure suggests that the pressure rise at the trailing edge of the boattail is not just a function of the total external-flow turning angle. Again, this result would be expected, since for the same free-stream Mach number the external flow on the boattails with different angle is at slightly different local Mach numbers and is flowing against different pressure gradients.

In figures 10 and 11, $\Delta C_{p,\beta_e}$, the ordinate, also partially determines the plume angle. If an investigator had a configuration similar to the ones in this investigation, he might assume several values of $\Delta C_{p,\beta_e}$, calculate ζ, and plot the coordinate values on figure 11. The point of intersection of the curve from the assumed values with the appropriate curve presented in figure 11 would represent a solution and would yield a value of $\Delta C_{p,\beta_e}$.

Even though the jet may greatly affect the pressures over a small portion of the boattail, it is the effect on drag that is of primary interest in the final analysis. Figures 12 to 16 present the boattail pressure-drag coefficients of the configurations tested. In figure 12 the jet-off pressure-drag coefficient is shown as a function of Mach number for a Mach number range of 0.3 to 2.2. The data for Mach numbers of 1.3 and below are from reference 1, and, as explained in reference 1, the level of the unfaired data near $M = 1.0$ is questionable because of possible effects of strut interference and reflected bow shock. The theoretical pressure-drag coefficients presented in the figure were obtained from pressure coefficients calculated by the method of characteristics and from

slender-body theory as described in reference 4. In the calculations by the method of characteristics it was assumed that free-stream conditions existed ahead of the boattail, an assumption slightly in error because at free-stream Mach numbers of 1.20 and 1.30 the local Mach numbers just ahead of the boattail were approximately 1.22 and 1.32, respectively. At free-stream Mach numbers of 1.83 and 2.20 the local Mach numbers just ahead of the boattail were not known. Agreement between the measured and theoretical values of drag is very good except for the slender-body theory at a boattail angle of 10°.

Figures 13 and 14 show the variation of the boattail pressure-drag coefficients with the jet exit static-pressure ratio and the jet total-pressure ratio for Mach numbers of 1.83 and 2.20. For the static-pressure ratios of the tests, the jet exhaust had very little effect on the boattail drag of the configurations with boattail angles of 3° and 5°. The drag of the configurations with boattail angles of 10° was affected much more by the jet. Also, for the configurations with boattail angles of 3° and 5°, the exit static-pressure ratio attains a value greater than 1 before the boattail drag starts to decrease with increasing pressure ratio. The pressure ratio necessary to make the boattail drag decrease is greater for a Mach number of 2.20 than for 1.83. Most noticeable from the data for the configurations with a boattail angle of 10° is the greater effect of the jet on the boattail drag at the lower Mach number. These last three effects could be expected from the pressure distributions (fig. 7).

Figure 15 shows the effect of Mach number on the incremental boattail pressure-drag coefficient (jet on minus jet off) due to jet operation at constant pressure ratios. The data at Mach numbers of 1.3 and lower are from reference 1. The figure illustrates again that through the supersonic Mach numbers tested, the magnitude of the jet effects tends to decrease as the Mach number increases. The jet affected the boattail drag most in the high subsonic to low supersonic speed range.

Figure 16 presents the variation of boattail pressure-drag coefficient with boattail flap length at several constant values of jet-exit static-pressure ratio. At Mach numbers of 1.83 and 2.20, for a constant boattail angle, the boattail drag continuously decreases as the nozzle is shortened. This effect was not always found at subsonic speeds (ref. 1), where shortening the boattail sometimes increased the drag by eliminating a portion of the boattail on which the pressures had recovered to values greater than those of the free stream. To obtain the total change in the afterbody force for a nozzle as it is shortened, changes in the internal performance have to be included.

It should be pointed out that these effects of the jet exhaust on the nozzle boattail pressures and drag are in the comparatively simple flow field of an isolated nacelle. In the more complicated flow field of a twin-engine configuration with interfairings the overall effects may be quite different, as shown in reference 5, because the local flow field for

each nozzle, which greatly influences the jet effects, is not axisymmetric and is strongly influenced by the interfairings between the nozzles.

CONCLUDING REMARKS

An investigation was conducted in the Langley 4- by 4-foot supersonic pressure tunnel to determine the jet effects on the boattail drag of nozzles with conical afterbodies. The results indicate that for the configurations tested, at Mach numbers of 1.83 and 2.20 and for jet-exit static-pressure ratios below 2.5, the influence of the exhaust on the boattail pressures is generally confined to a small area at the downstream end of the boattail. This finding is in contrast to results for subsonic speeds, at which the jet frequently influenced the pressures over the entire length of the boattail. Also, the jet-exit static-pressure ratio generally must be well above 1 before the trailing-edge pressure is affected by the jet.

The jet exhaust generally had a greater influence on the boattail pressures, and therefore on drag, at a Mach number of 1.83 than at 2.20. Jet interference was more pronounced for the configurations with boattail angles of 10° than for those with boattail angles of 3° and 5°.

At supersonic speeds, shortening the boattail always reduced boattail drag for a given static-pressure ratio.

Langley Research Center,
National Aeronautics and Space Administration,
Hampton, Va., June 15, 1972.

APPENDIX

STANDARD NOZZLE WITH CIRCULAR-ARC BOATTAIL

An exhaust nozzle with a circular-arc boattail and geometry that conformed to recommendations of the Supersonic Tunnel Association (S.T.A.) for a standard nozzle was tested on the air-powered nacelle to provide data for comparison with data from other tunnels on nozzles of the same configuration. A sketch of this nozzle with its orifice locations is shown in figure 17. The jet total pressure for the standard nozzle was the average measurement of the five internal rake tubes.

Jet-off boattail pressure-coefficient distributions for the circular-arc nozzle are presented in figures 18 and 19. Figure 18 shows that the pressures on the bottom of the nozzle are affected by the strut wake; therefore, as in the body of the report, only the pressures on the top are used for further comparisons, calculations of drag, and so forth. The pressure coefficients for the top row of orifices and those computed by the method of characteristics (fig. 19) agree very well except near the trailing edge, where there is a shock on the boattail.

The variation with free-stream Mach number of the jet-off boattail pressure-drag coefficient of the standard nozzle is presented in figure 20 (the data at Mach numbers of 1.3 and below are from ref. 1). The theoretical drag coefficients shown in the figure were obtained from boattail pressure coefficients calculated by the method of characteristics and from slender-body theory as described in reference 4. The calculated values do not agree very well with the drag coefficients obtained from the measured pressures because of the shock near the end of the boattail in the real flow. The application of slender-body theory is further handicapped by the steepness of the boattail, which begins to violate the assumption of that theory.

Figure 21 presents the boattail pressure-coefficient distributions on the standard nozzle for several values of jet pressure ratio. Both the total-pressure ratios and exit static-pressure ratios are indicated. The effect of the jet exhaust on the boattail pressures is similar to the effects for the conical-boattail nozzles discussed in the main part of the report.

In figure 22 the boattail pressure-drag coefficient of the standard nozzle is presented as a function of the jet total-pressure ratio and of the jet-exit static-pressure ratio.

REFERENCES

1. Compton, William B., III; and Runckel, Jack F.: Jet Effects on the Boattail Axial Force of Conical Afterbodies at Subsonic and Transonic Speeds. NASA TM X-1960, 1970.

2. Ames Research Staff: Equations, Tables, and Charts for Compressible Flow. NACA Rep. 1135, 1953. (Supersedes NACA TN 1428.)

3. Putnam, Lawrence E.; and Capone, Francis J.: Experimental Determination of Equivalent Solid Bodies to Represent Jets Exhausting Into a Mach 2.20 External Stream. NASA TN D-5553, 1969.

4. Harris, Roy V., Jr.: An Analysis and Correlation of Aircraft Wave Drag. NASA TM X-947, 1964.

5. Lee, Edwin E., Jr.; and Runckel, Jack F.: Performance of Closely Spaced Twin-Jet Afterbodies With Different Inboard-Outboard Fairing and Nozzle Shapes. NASA TM X-2329, 1971.

TABLE I.- NOZZLE SURFACE ORIFICE LOCATIONS

ϕ, deg	Nondimensionalized axial distance from boattail corner to orifice, x/d_m, for –			
	Boattails with $l/d_m = 1.0$; $\beta = 3^o$, 5^o, and 10^o	Boattails with $l/d_m = 0.8$		Boattails with $l/d_m = 0.6$; $\beta = 3^o$, 5^o, and 10^o
		$\beta = 3^o$ and 5^o	$\beta = 10^o$	
0 and 90	-0.02	-0.02	-0.02	-0.02
	.02	.02	.02	.02
	.08	.08	.08	.08
	.25	.20	.20	.15
	.50	.40	.40	.30
	.75	.60	.60	.45
	.97	.78	.77	.58
45, 135, 157.5, and 180	.02	.02	.02	.02
	.25	.20	.20	.15
	.50	.40	.40	.30
	.75	.60	.60	.45
	.97	.78	.77	.58

TABLE II.- NOZZLE DIVERGENT-WALL ORIFICE LOCATIONS; $\phi = 337.5^o$

Nondimensionalized axial distance from nozzle throat to orifice, f/d_m, for –							
Boattails with $l/d_m = 1.0$		Boattails with $l/d_m = 0.8$			Boattails with $l/d_m = 0.6$		
$\beta = 3^o$	$\beta = 5^o$ and 10^o	$\beta = 3^o$	$\beta = 5^o$	$\beta = 10^o$	$\beta = 3^o$	$\beta = 5^o$	$\beta = 10^o$
0.17	0.17	0.17	0.17	0.15	0.17	0.16	0.17
.33	.33	.34	.34	.32	.34	.33	.34
.50	.50	.50	.50	.48	.50	.49	.42
.67	.67	.67	.67	.65	.66	.66	.50
.83	.83	.75	.75	.73	.75	.74	.59
.91	.92	.83	.84	.82	.83	.83	.67
1.00	1.00	.92	.92	.90	.91	.91	.75
1.08	1.08	1.00	1.00	.98			.84
1.16	1.17	1.08	1.08	1.07			.92

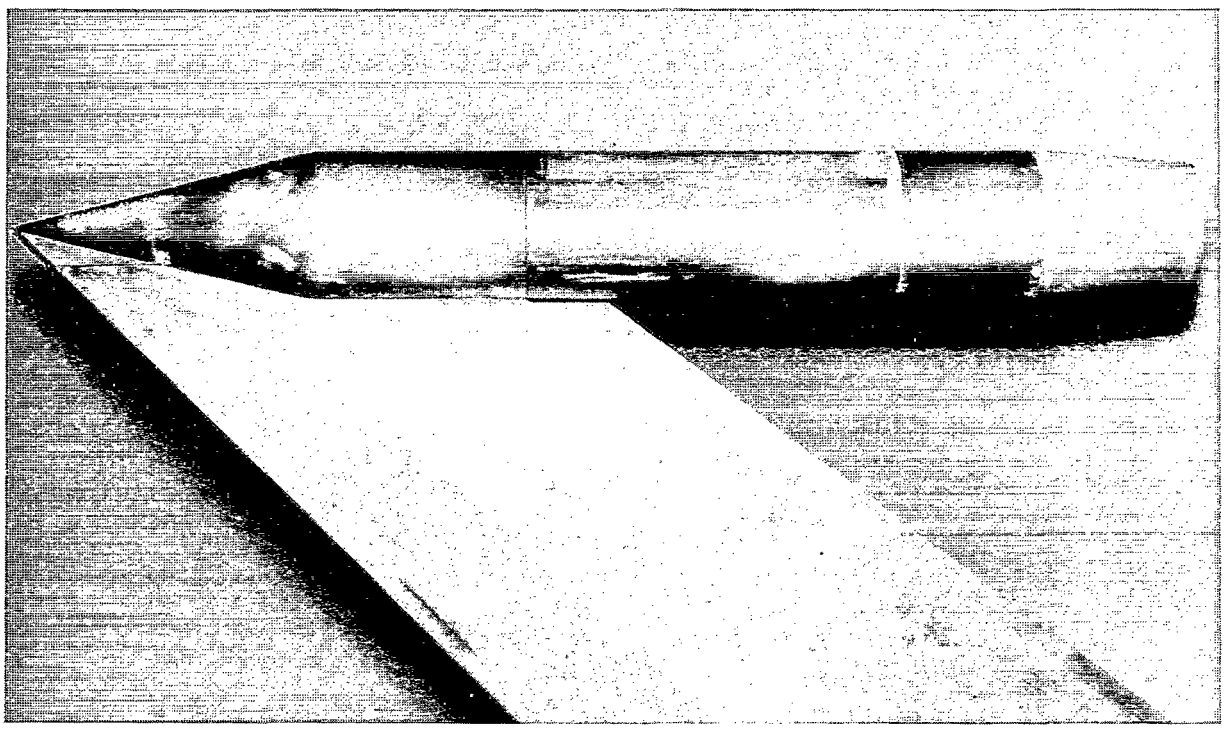

L-67-1987

Figure 1.- Photograph of model having nozzle with $l/d_m = 1.0$ and $\beta = 5^o$.

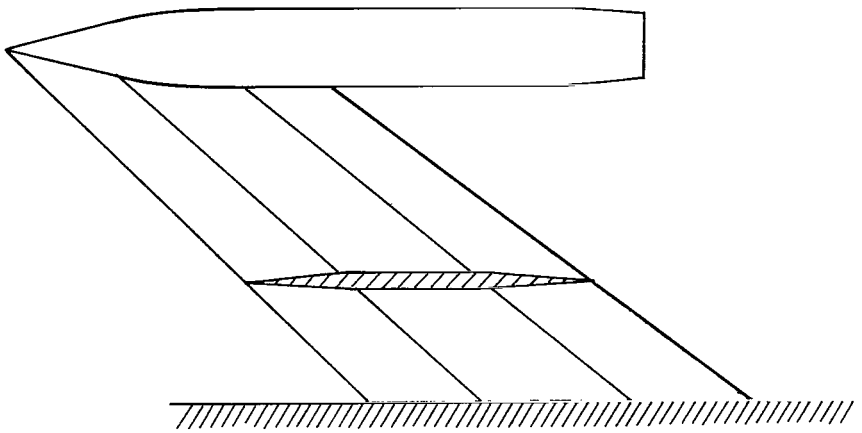

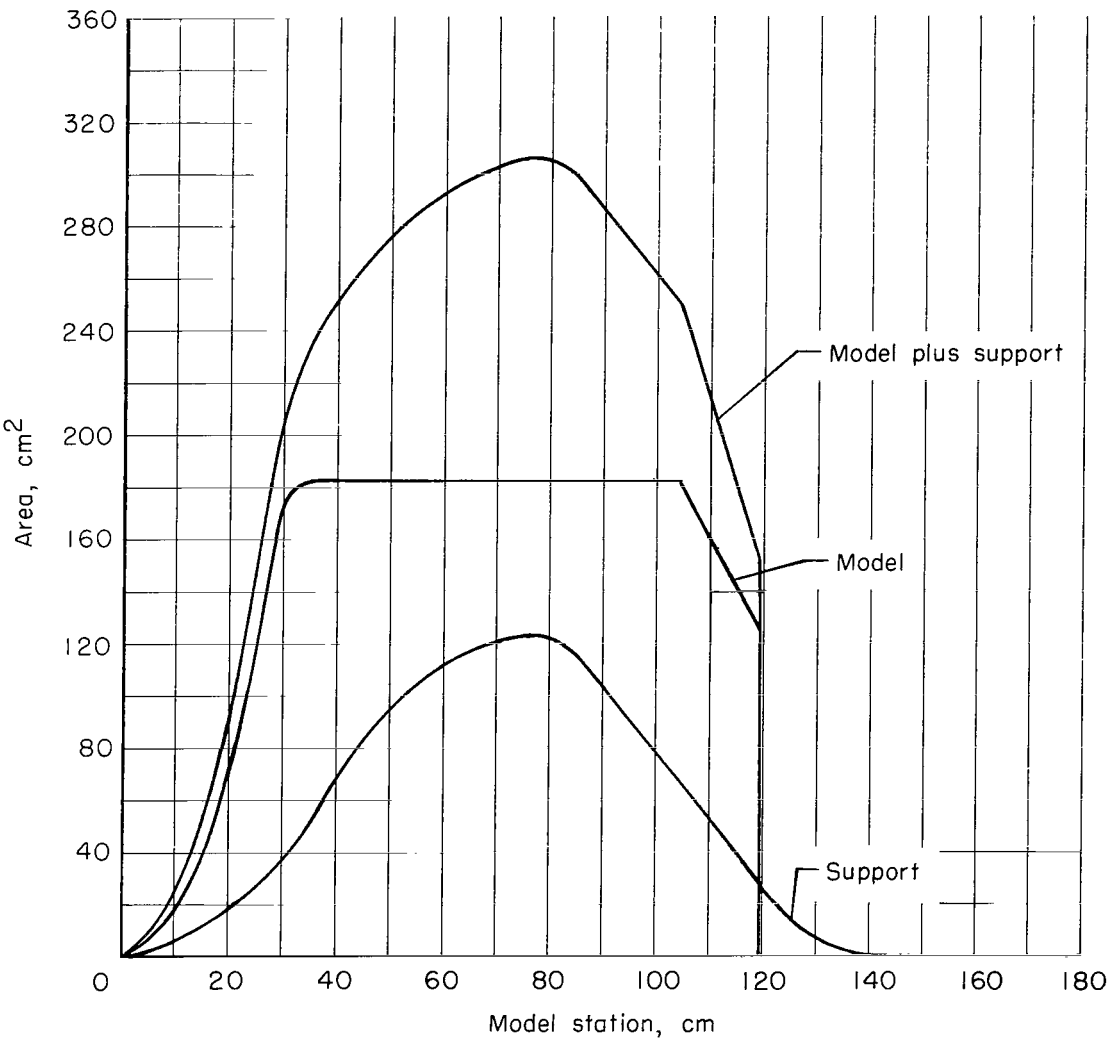

Figure 2.- Cross-section area distributions of support strut and model with an afterbody having a boattail angle β of 5^{o}.

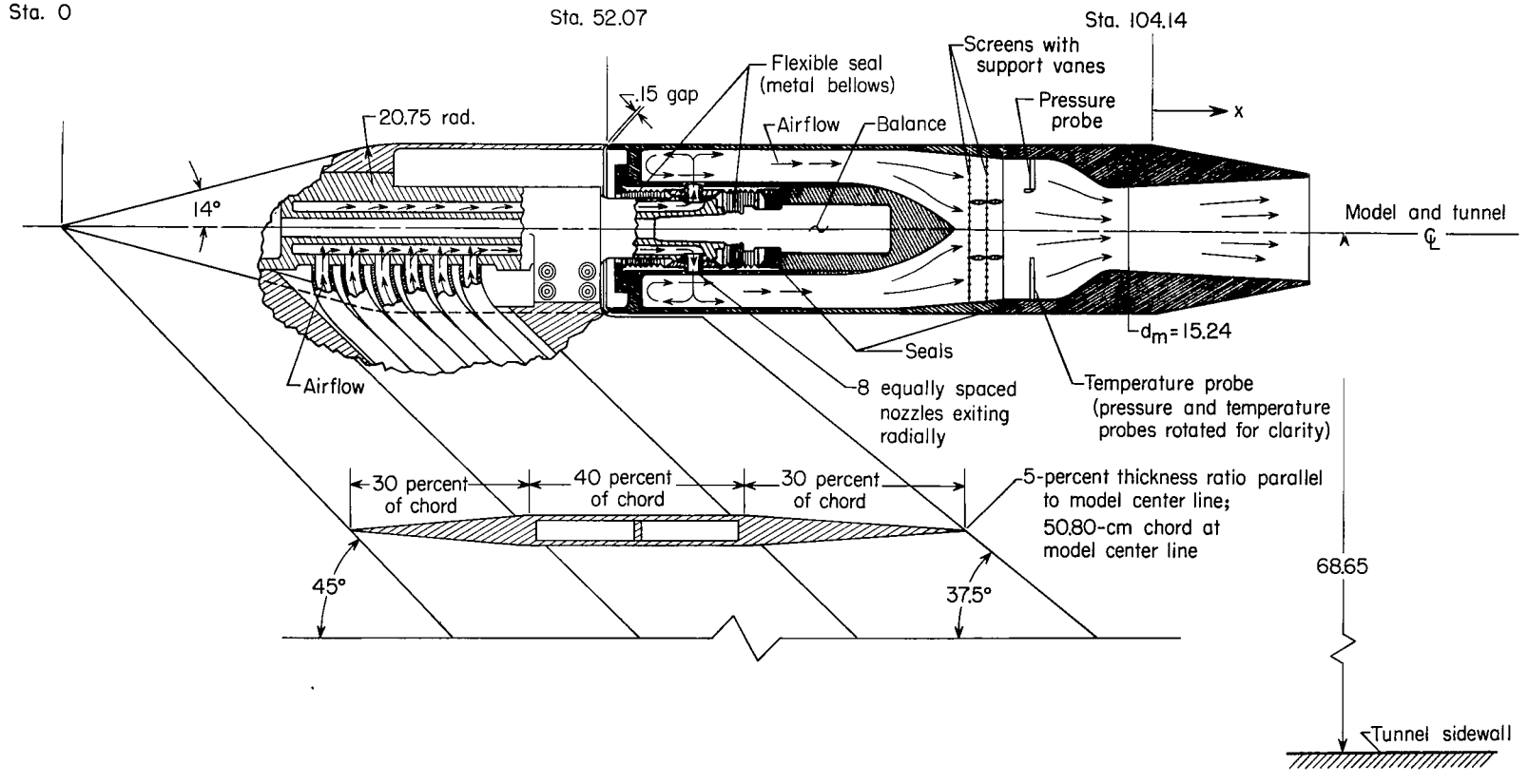

Figure 3.- Sketch of air-powered nacelle model with typical nozzle configuration installed. All dimensions are in centimeters unless otherwise noted.

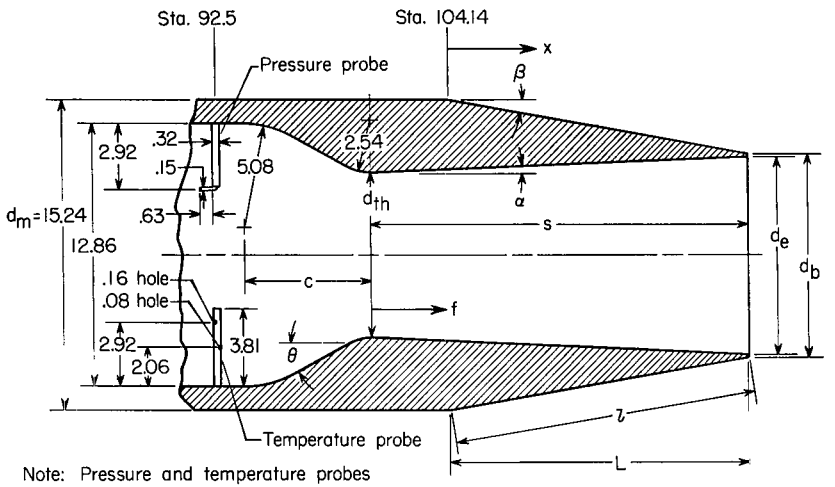

Note: Pressure and temperature probes shown rotated out of position for clarity in side view.

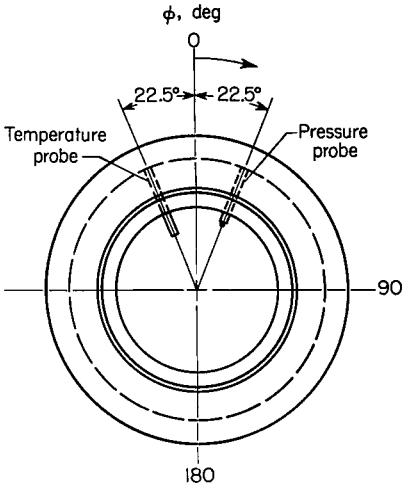

Configuration	Type nozzle	Design dimensions												
		l/d_m	β, deg	L/d_m	d_b/d_m	A_b/A_m	A_e/A_b	A_{th}/A_m	ϵ_e	s/d_{th}	α, deg	c/d_{th}	θ, deg	$(p_{t,j}/p_\infty)_{des}$
* 1	Super. cruise	1.0	0	1.000	1.000	1.000	0.970	0.247	3.925	2.444	11.5	0.860	30	32.60
* 2	Max. aug.	1.0	0	1.000	1.000	1.000	.970	.454	2.139	1.826	7.2	.484	20	11.95
3	↓	1.0	3.00	1.000	.895	.802	.970	.452	1.716	1.840	4.8	.485	20	8.08
4		1.0	5.02	.996	.825	.681	.965	.445	1.460	1.846	3.2	.485	20	5.91
5		1.0	10.00	.985	.653	.426	.955	.366	1.111	2.049	.8	.689	20	3.14
* 6	Sub. cruise	1.0	15.00	.966	.482	.233	.939	.218	1.087	2.765	.4	1.063	30	2.94
* 7	Super. cruise	.8	0	.800	1.000	1.000	.970	.293	3.307	2.045	11.5	.487	30	24.80
* 8	Max. aug.	.8	0	.800	1.000	1.000	.970	.454	2.135	1.659	8.0	.477	20	11.95
9		.8	3.30	.800	.916	.839	.968	.452	1.795	1.670	5.8	.487	20	8.77
10	↓	.8	5.00	.797	.861	.741	.965	.450	1.589	1.678	4.4	.486	20	6.98
11		.8	10.00	.788	.722	.521	.959	.450	1.111	1.682	.9	.486	20	3.14
* 12	Sub. cruise	.8	15.00	.773	.586	.343	.950	.300	1.086	2.062	.6	.712	30	2.94
* 13	Super. cruise	.6	0	.600	1.000	1.000	.970	.360	2.695	1.627	11.5	.530	30	17.70
* 14	Max. aug.	.6	0	.600	1.000	1.000	.970	.455	2.156	1.459	9.1	.474	20	11.95
15	↓	.6	3.00	.599	.937	.878	.968	.453	1.876	1.468	7.2	.480	20	9.52
16		.6	5.00	.598	.895	.802	.967	.450	1.722	1.477	6.0	.482	20	8.14
17		.6	10.00	.590	.792	.627	.962	.451	1.340	1.482	3.0	.484	20	4.92
* 18	Sub. cruise	.6	15.00	.580	.698	.475	.957	.350	1.300	1.682	2.4	.595	30	4.62
* 19	↓	.6	7.50	.595	.843	.711	.642	.350	1.300	1.709	2.4	.465	30	4.62
* 20		.6	20.00	.564	.590	.347	.950	.330	1.186	1.637	.8	.703	30	3.74
* 21		.638	15.00	.616	.670	.449	.956	.395	1.087	1.628	.7	.510	30	2.94

* Not tested in this investigation

Figure 4.- Geometry and dimensions of variable-flap nozzle configurations. All dimensions are in centimeters unless otherwise noted.

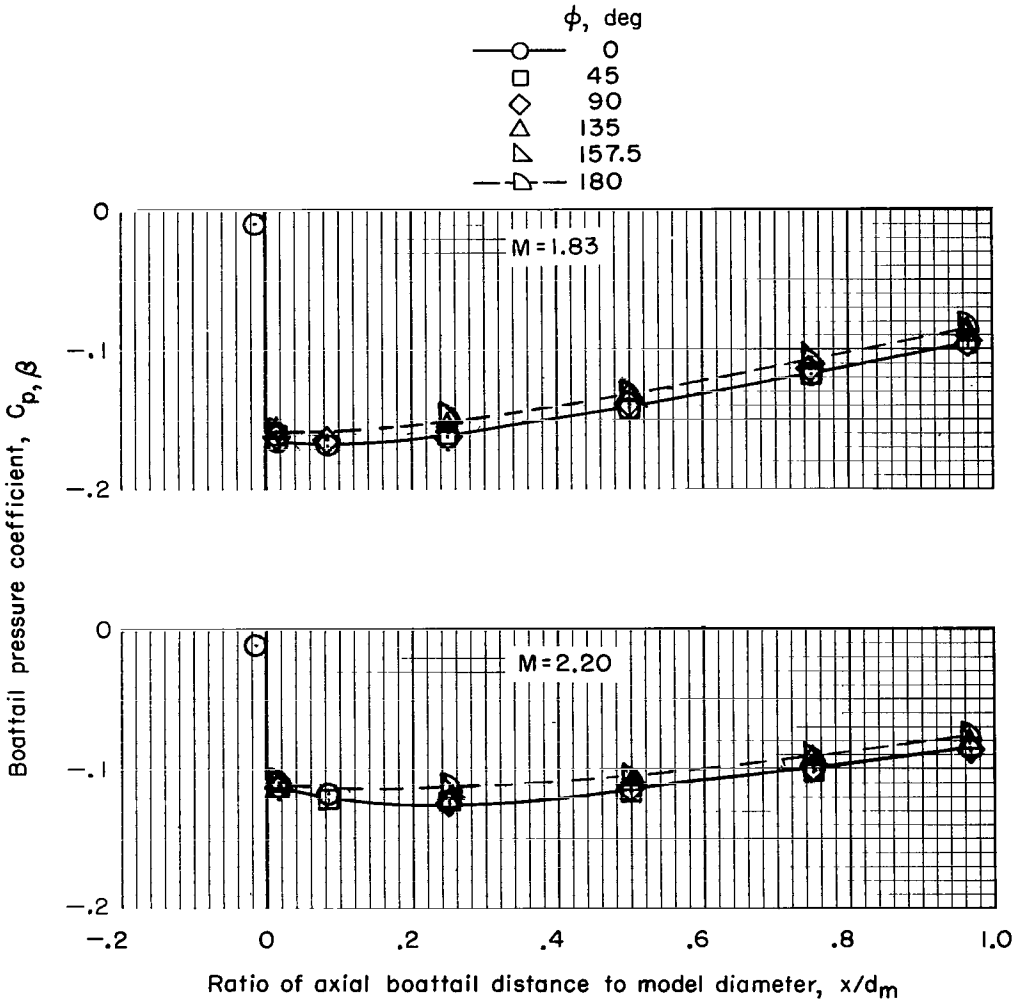

Figure 5.- Boattail pressure coefficient distributions for several values of ϕ. Jet off; $\beta = 10^{o}$; $l/d_m = 1.0$.

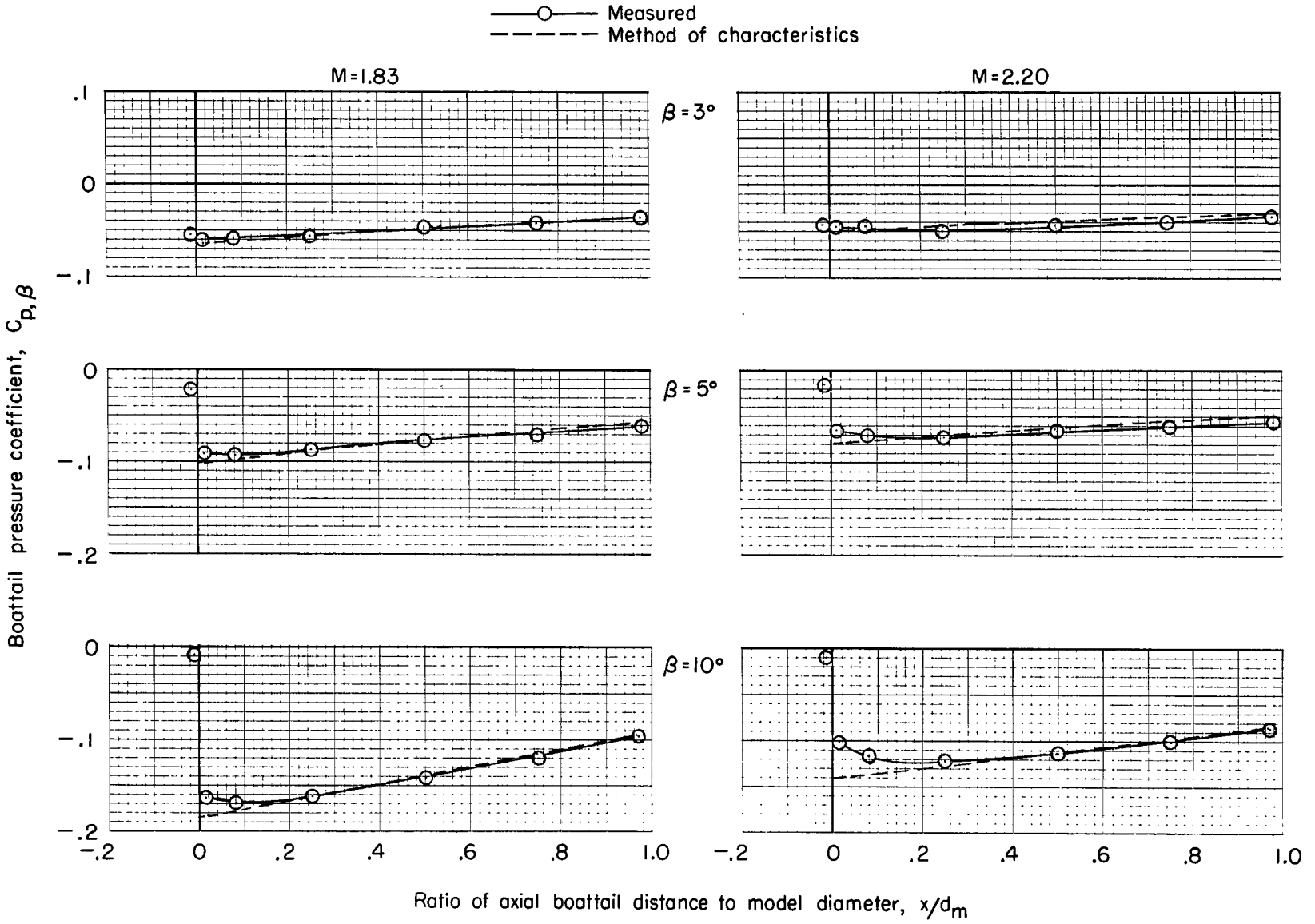

Figure 6.- Comparison of measured boattail pressure distributions with those computed by the method of characteristics. $l/d_m = 1.0$; $\phi = 0^o$; jet off.

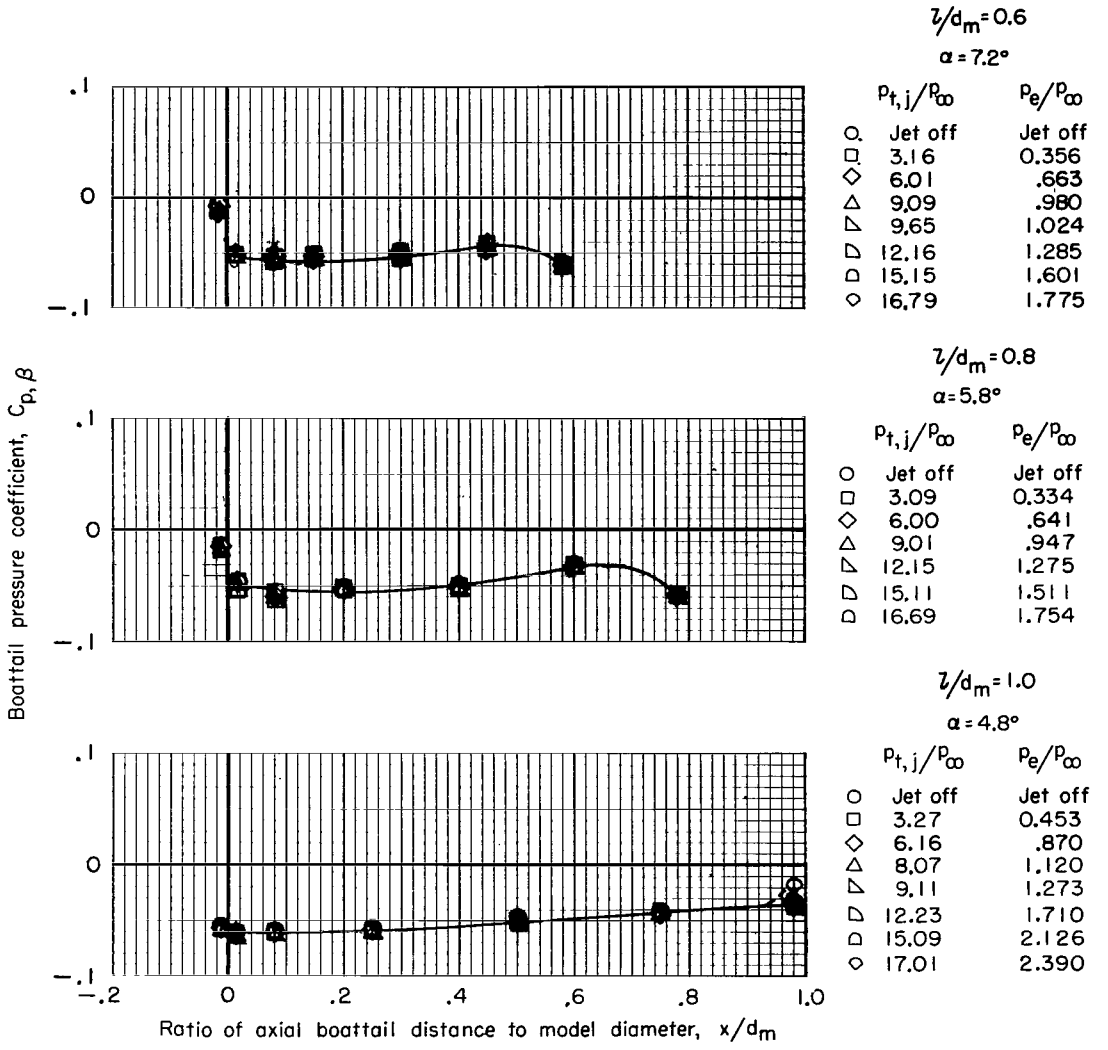

(a) $\beta \approx 3^o$; M = 1.83.

Figure 7.- Boattail pressure-coefficient distributions for various values of jet pressure ratio. $\phi = 0^o$. Missing values of p_e/p_∞ indicate that the measurement of p_e was in error.

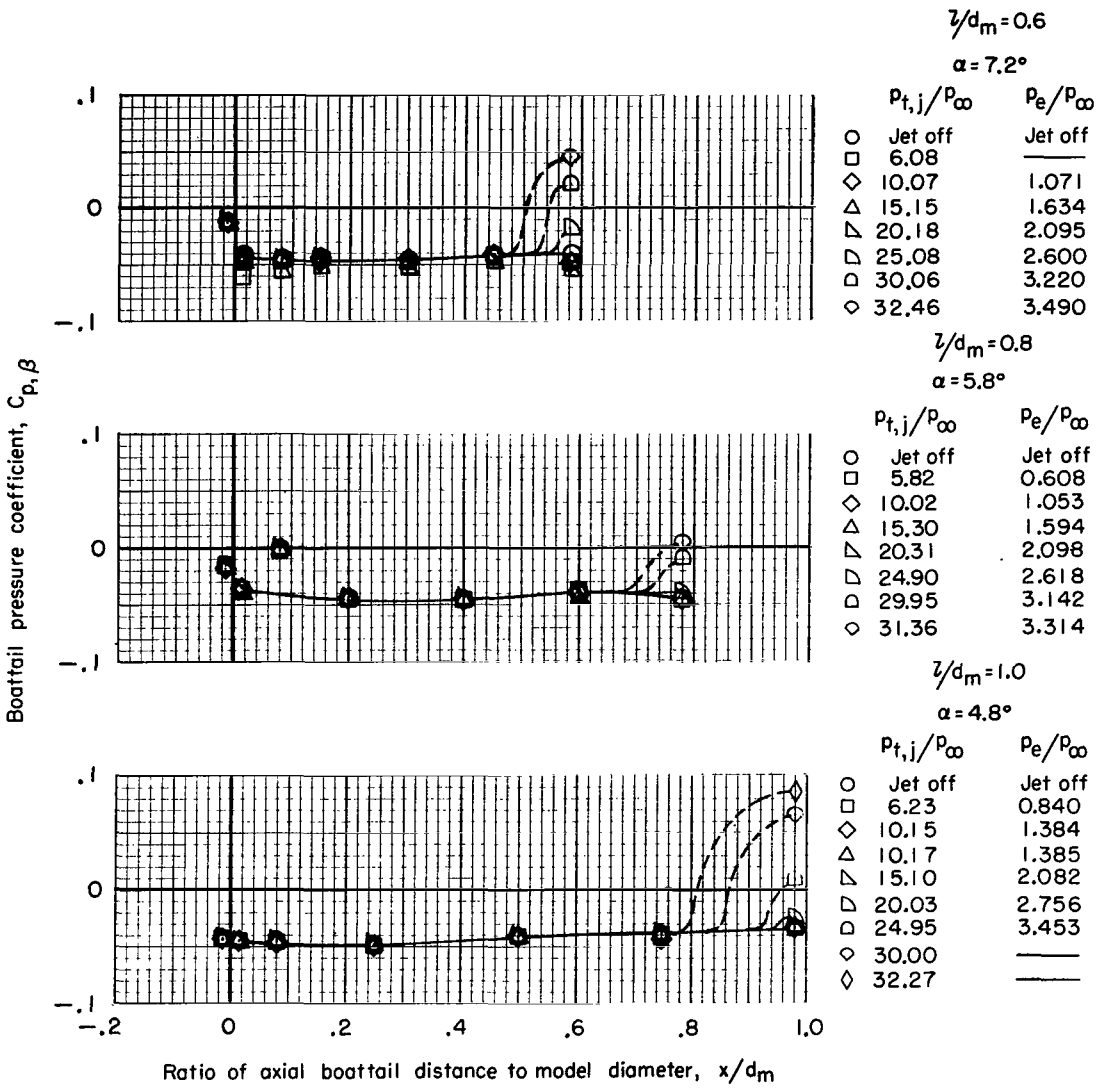

(b) $\beta \approx 3^o$; M = 2.2.

Figure 7.- Continued.

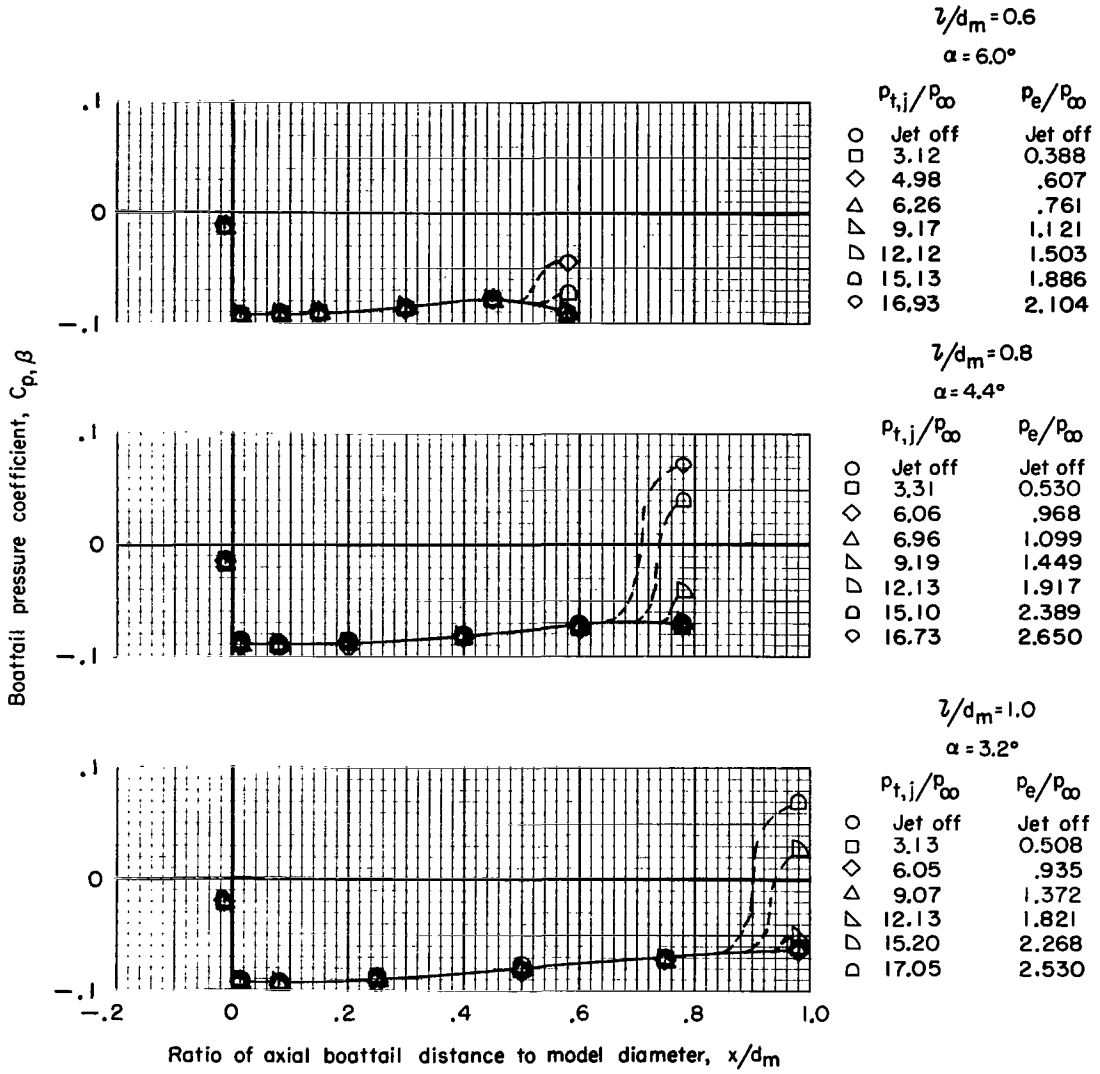

(c) $\beta = 5^o$; M = 1.83.

Figure 7.- Continued.

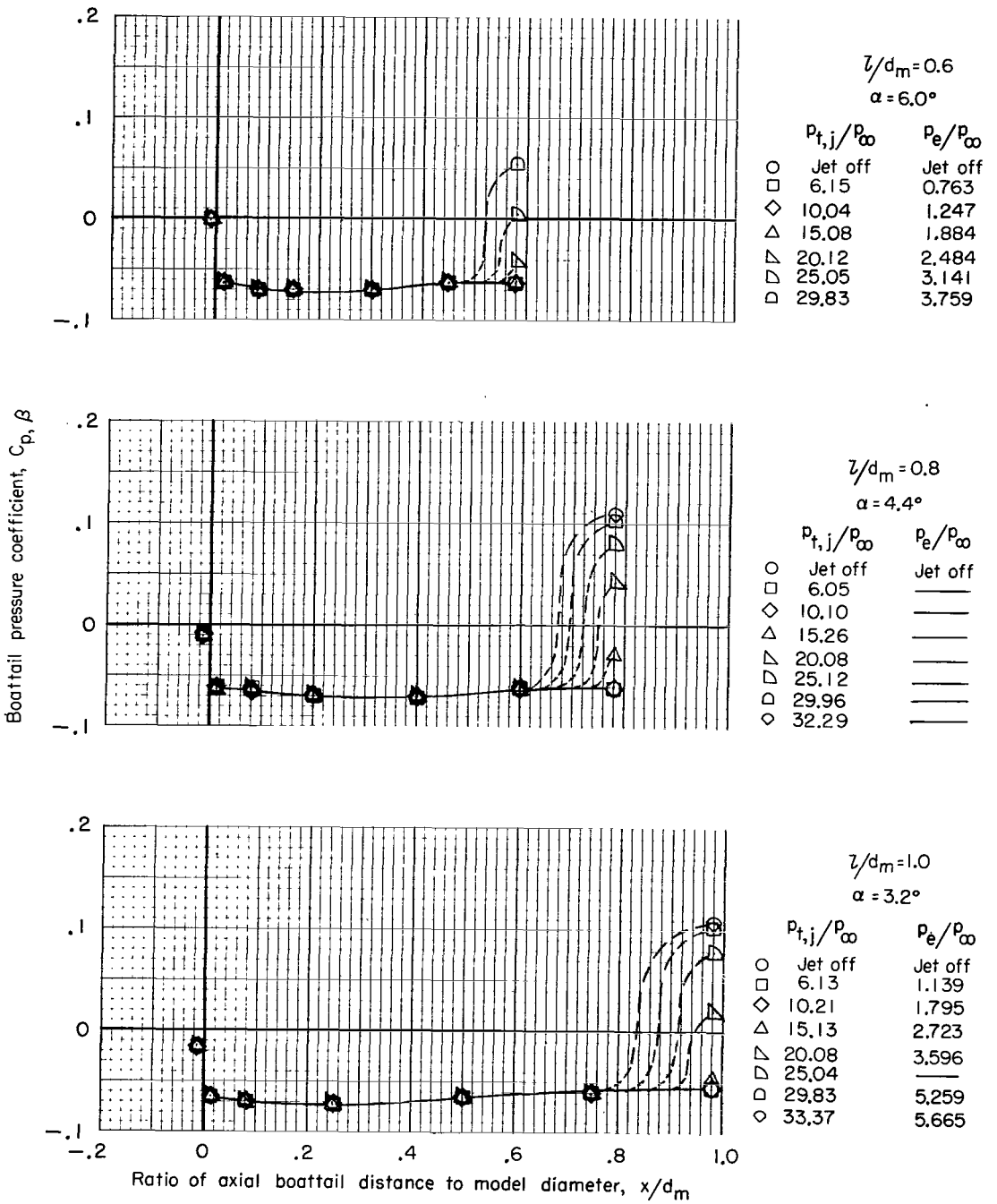

(d) $\beta = 5^o$; M = 2.2.

Figure 7.- Continued.

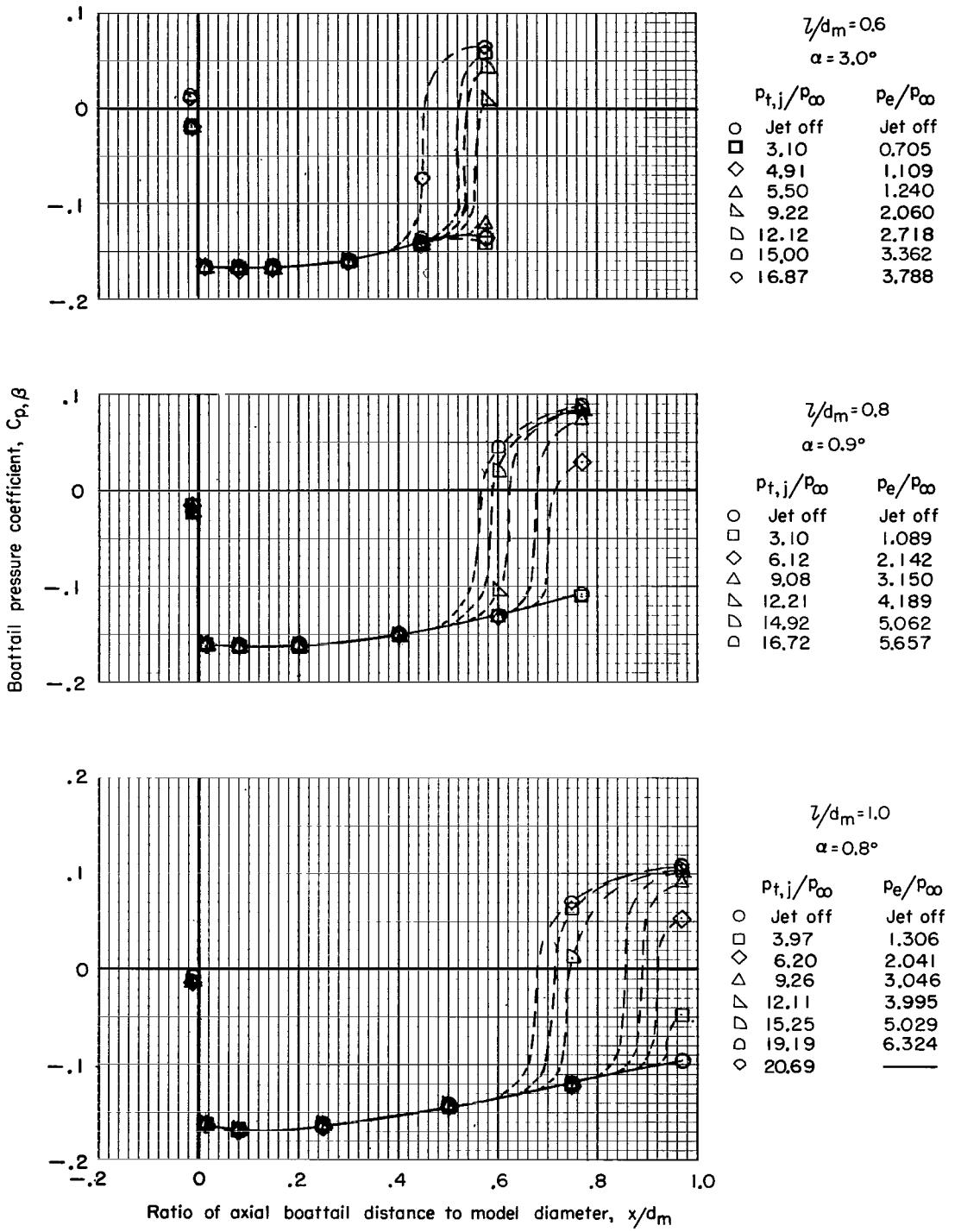

(e) $\beta = 10^o$; M = 1.83.

Figure 7.- Continued.

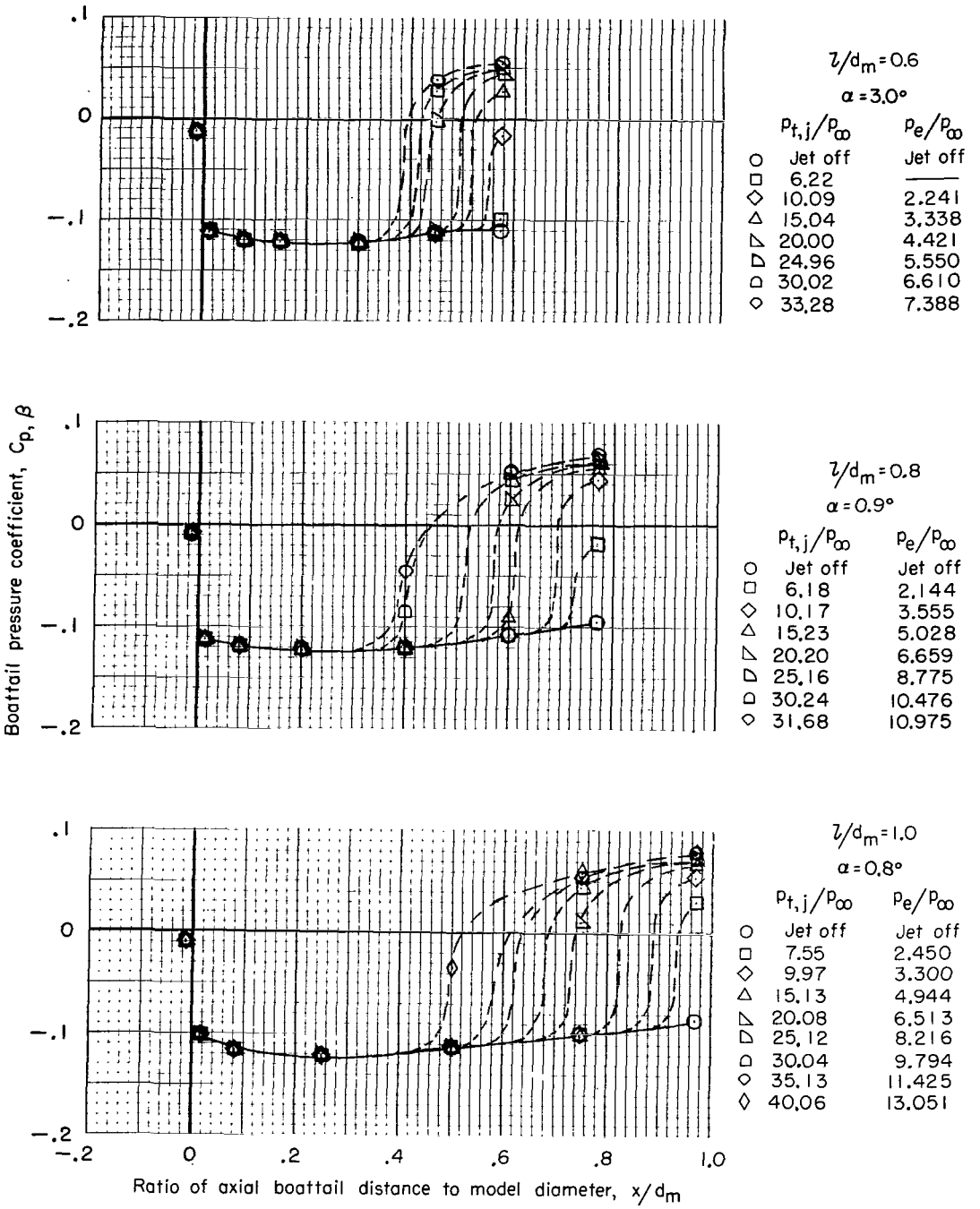

(f) $\beta = 10^o$; M = 2.2.

Figure 7.- Concluded.

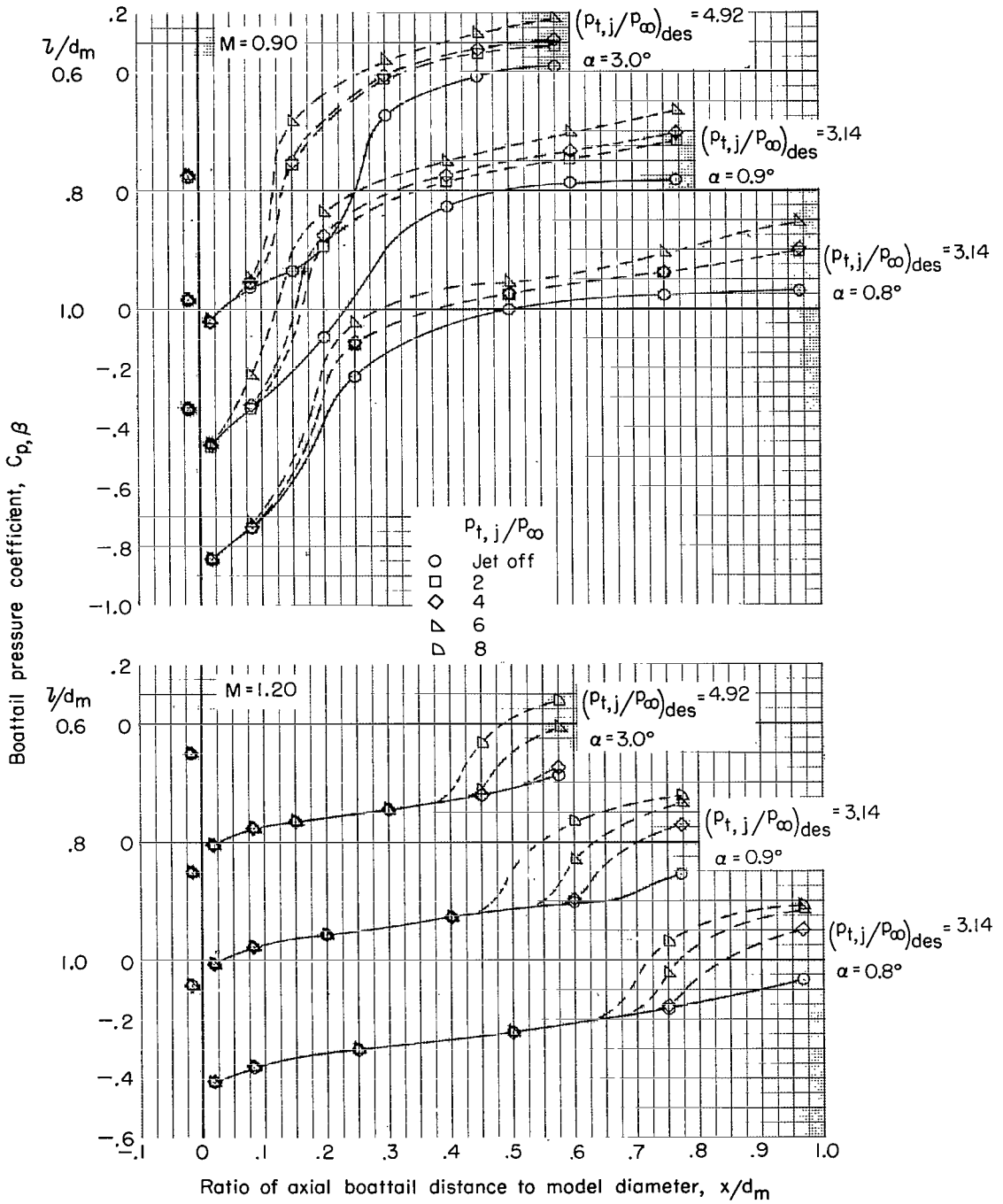

Figure 8.- Boattail pressure distributions at various pressure ratios for nozzles with boattail angles of 10^o. $\phi = 0^o$. (From ref. 1.)

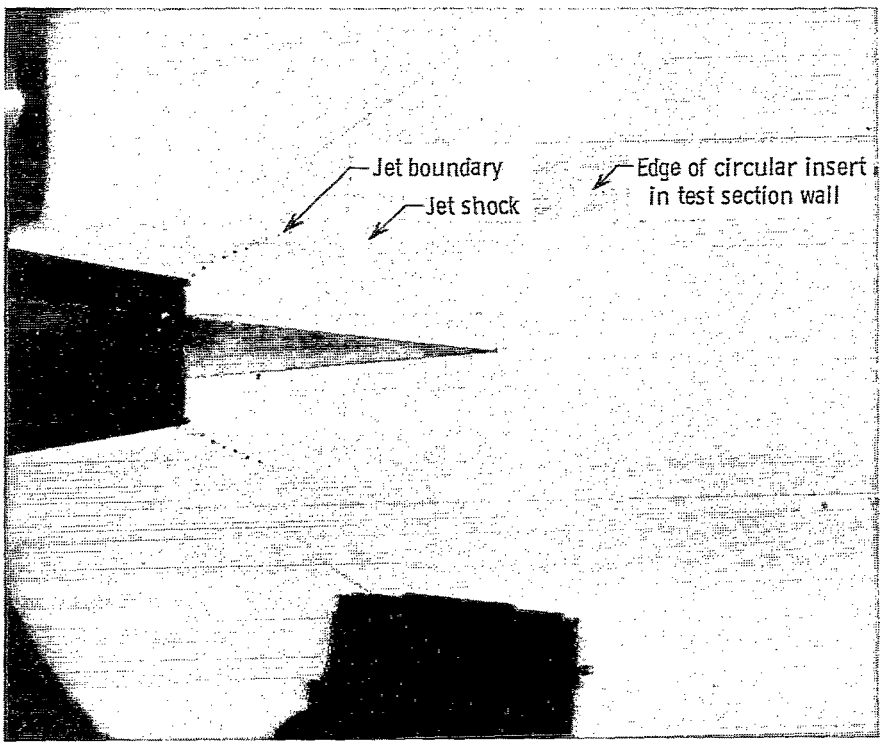

L-72-2430

(a) Shadowgraph. $p_{t,j}/p_\infty = 40.06$; $p_e/p_\infty = 13.051$; $\alpha = 0.8^o$; $M = 2.20$; $\beta = 10^o$; $\ell/d_m = 1.0$.

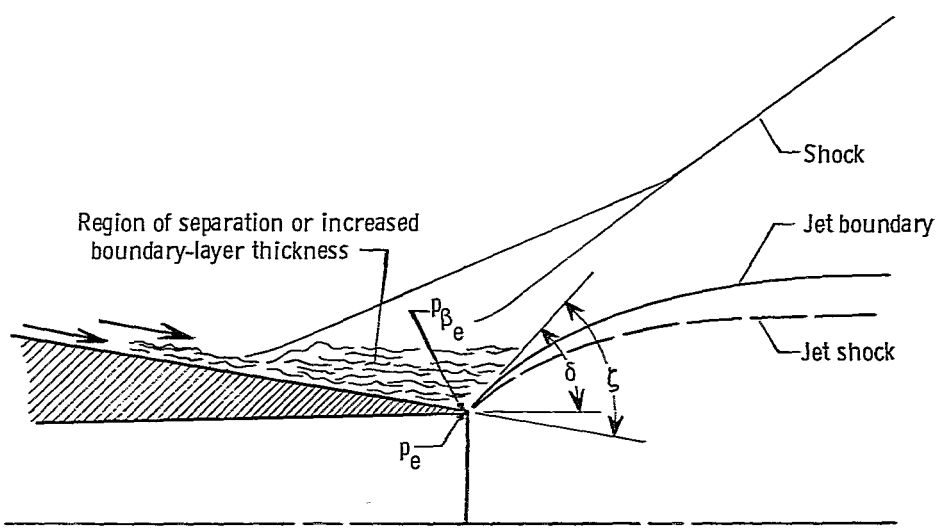

(b) Sketch.

Figure 9.- Flow field in vicinity of nozzle exit with an underexpanded jet.

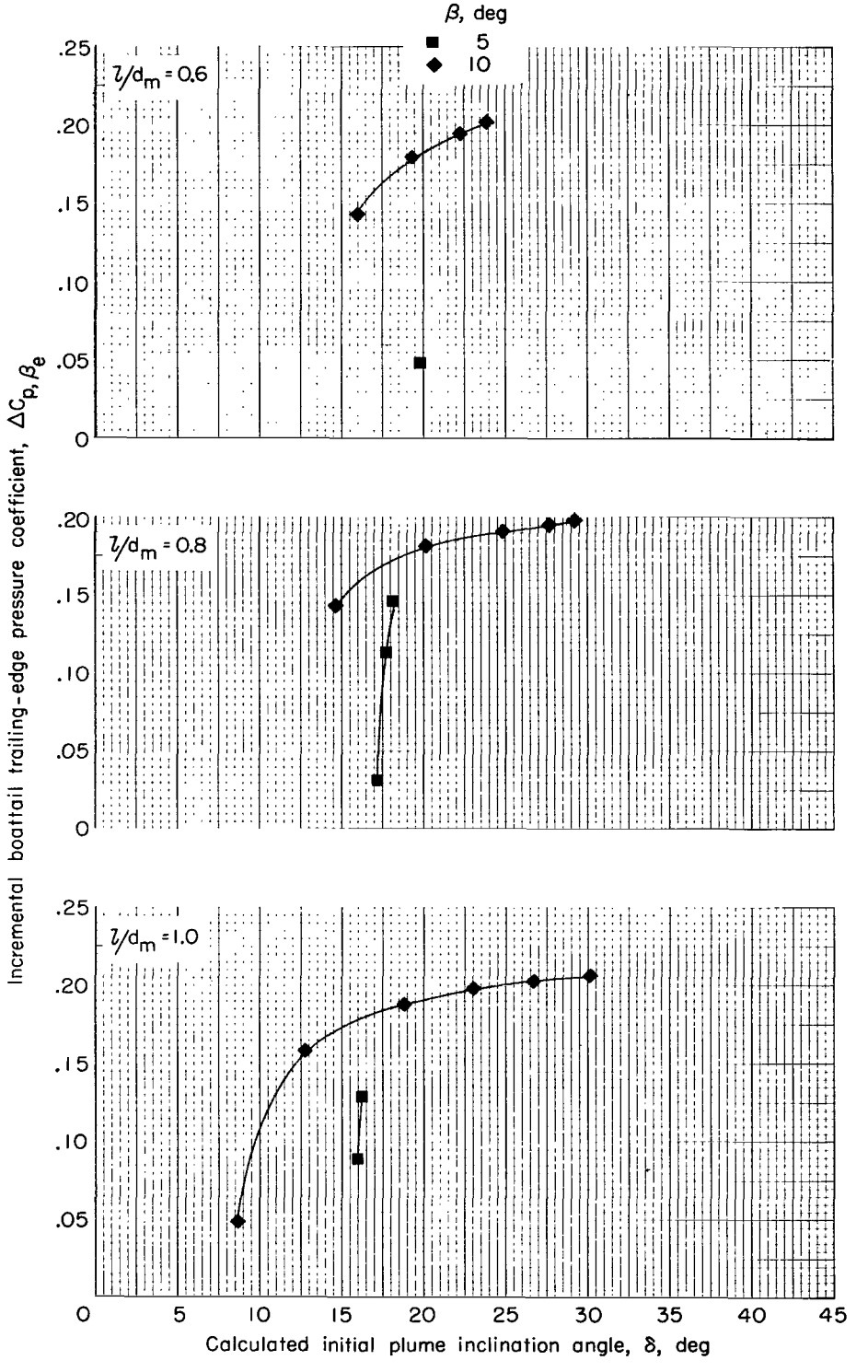

(a) M = 1.83.

Figure 10.- Effect of initial plume inclination angle on the incremental boattail trailing-edge pressure coefficient.

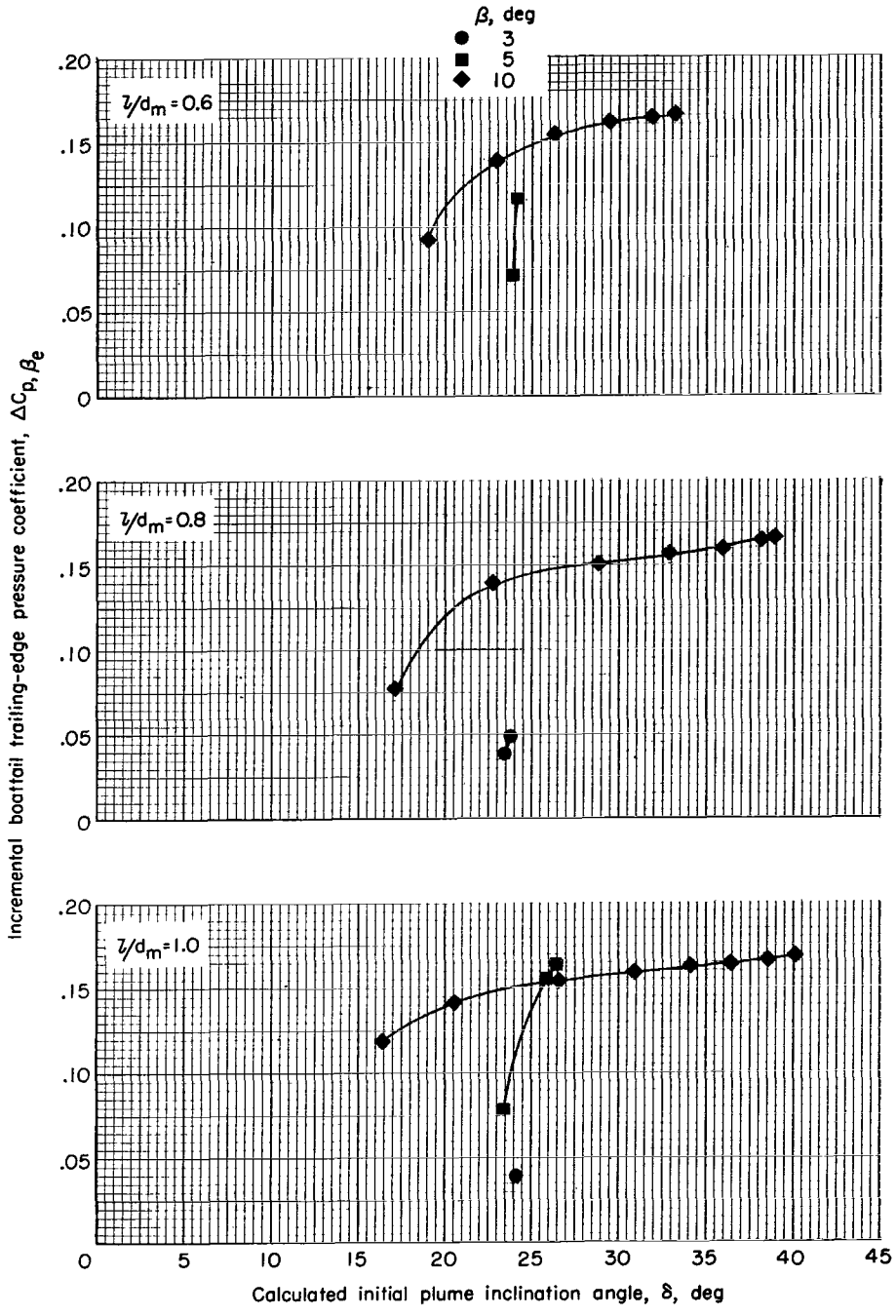

(b) M = 2.20.

Figure 10.- Concluded.

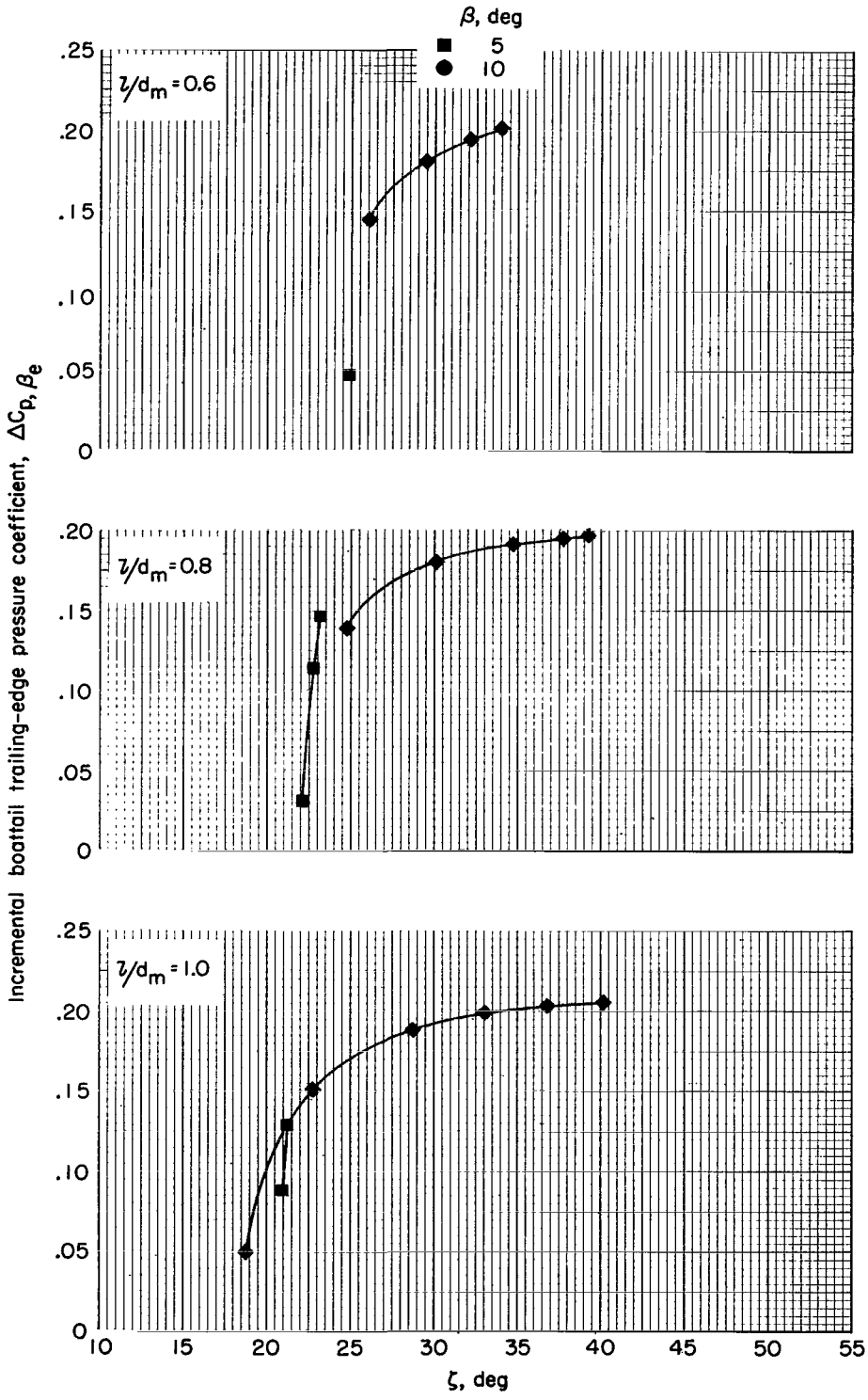

(a) M = 1.83.

Figure 11.- Effect of hypothetical boattail flow turning angle on the incremental boattail trailing-edge pressure coefficient. $\zeta = \delta + \beta$.

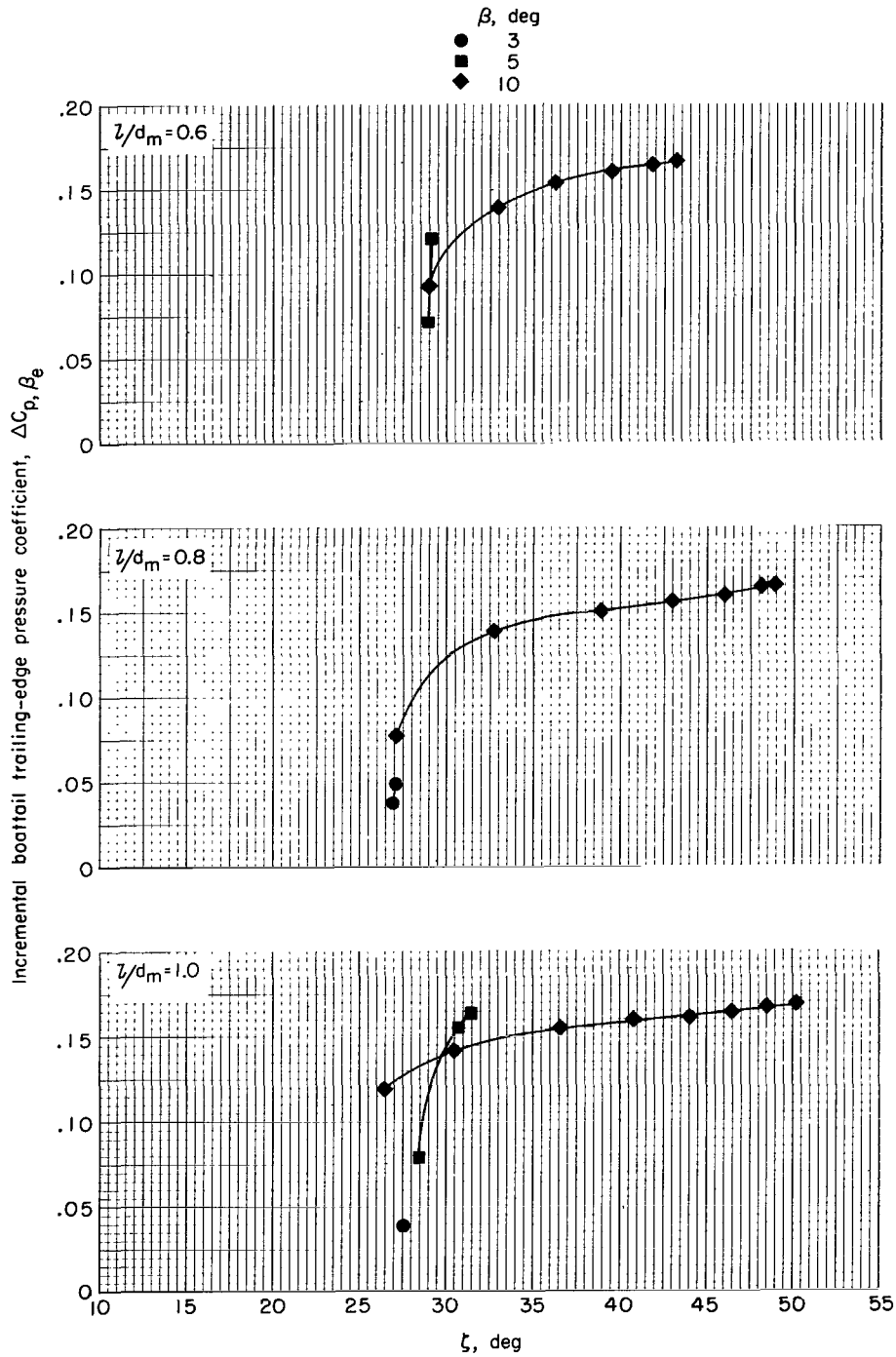

(b) M = 2.20.

Figure 11.- Concluded.

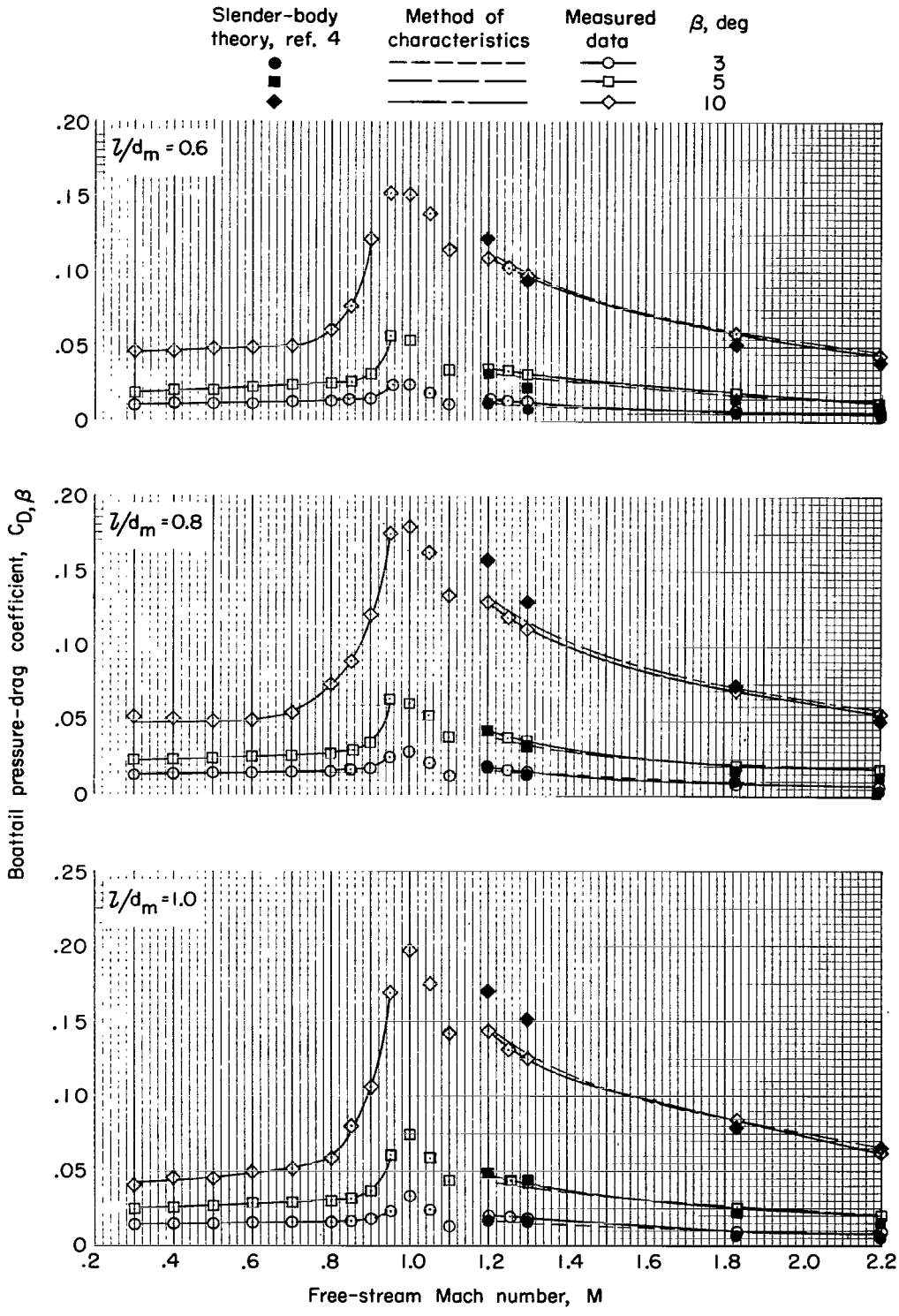

Figure 12.- Variation of jet-off boattail pressure-drag coefficient with Mach number.

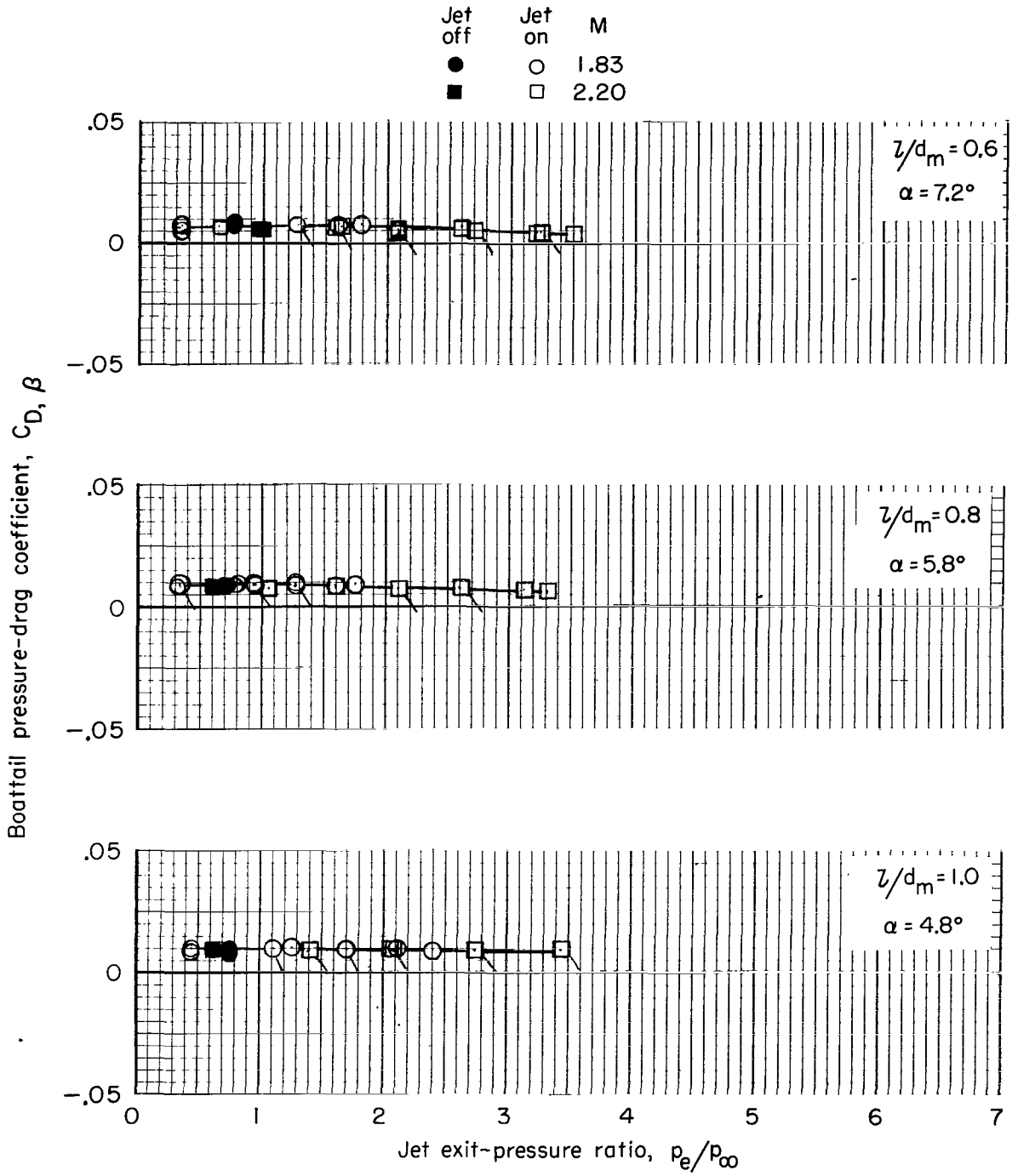

(a) $\beta \approx 3^o$.

Figure 13.- Variation of boattail pressure-drag coefficient with jet-exit static-pressure ratio. Flagged symbols indicate data taken as pressure ratio was decreased.

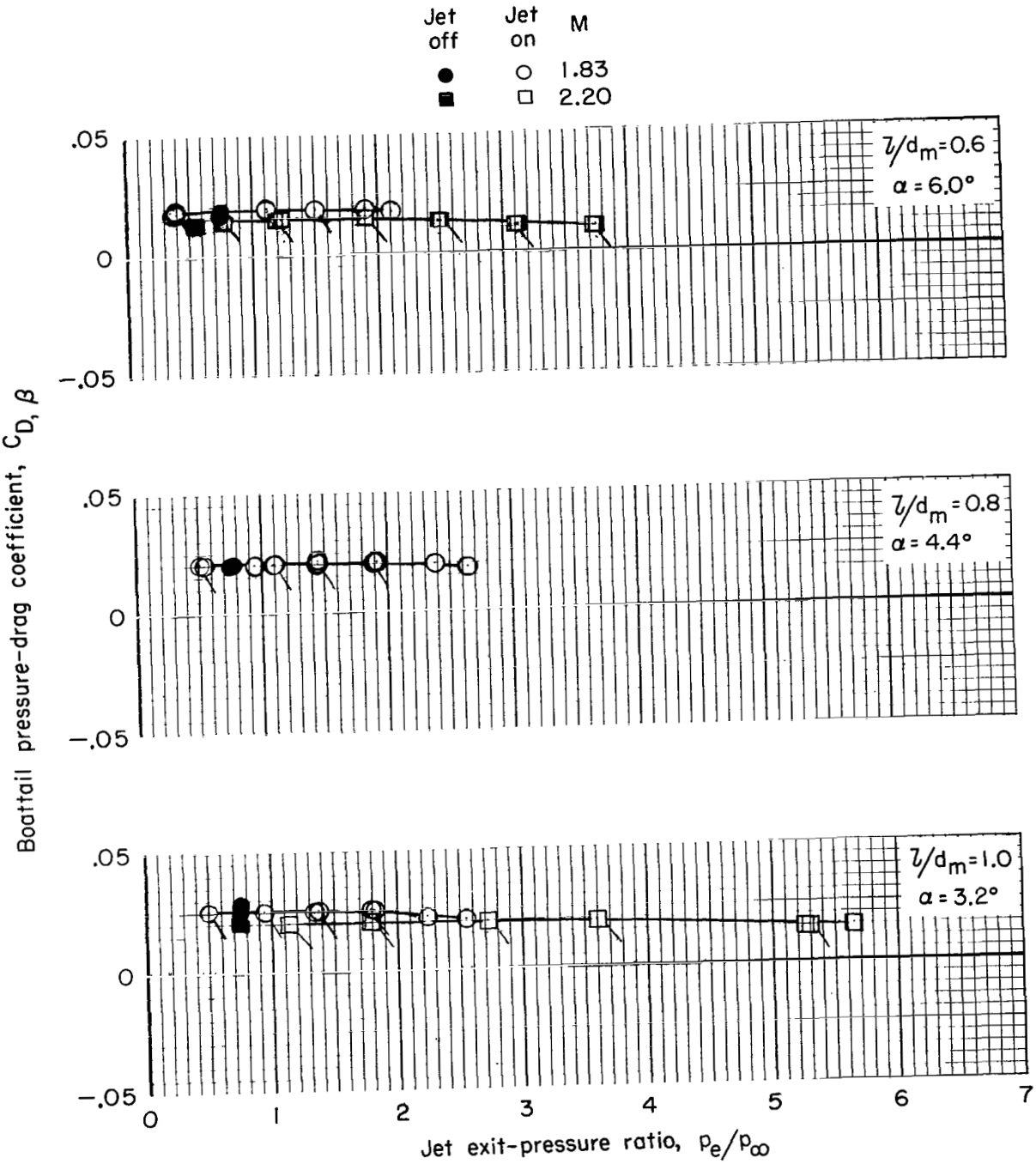

(b) $\beta = 5^o$.

Figure 13.- Continued.

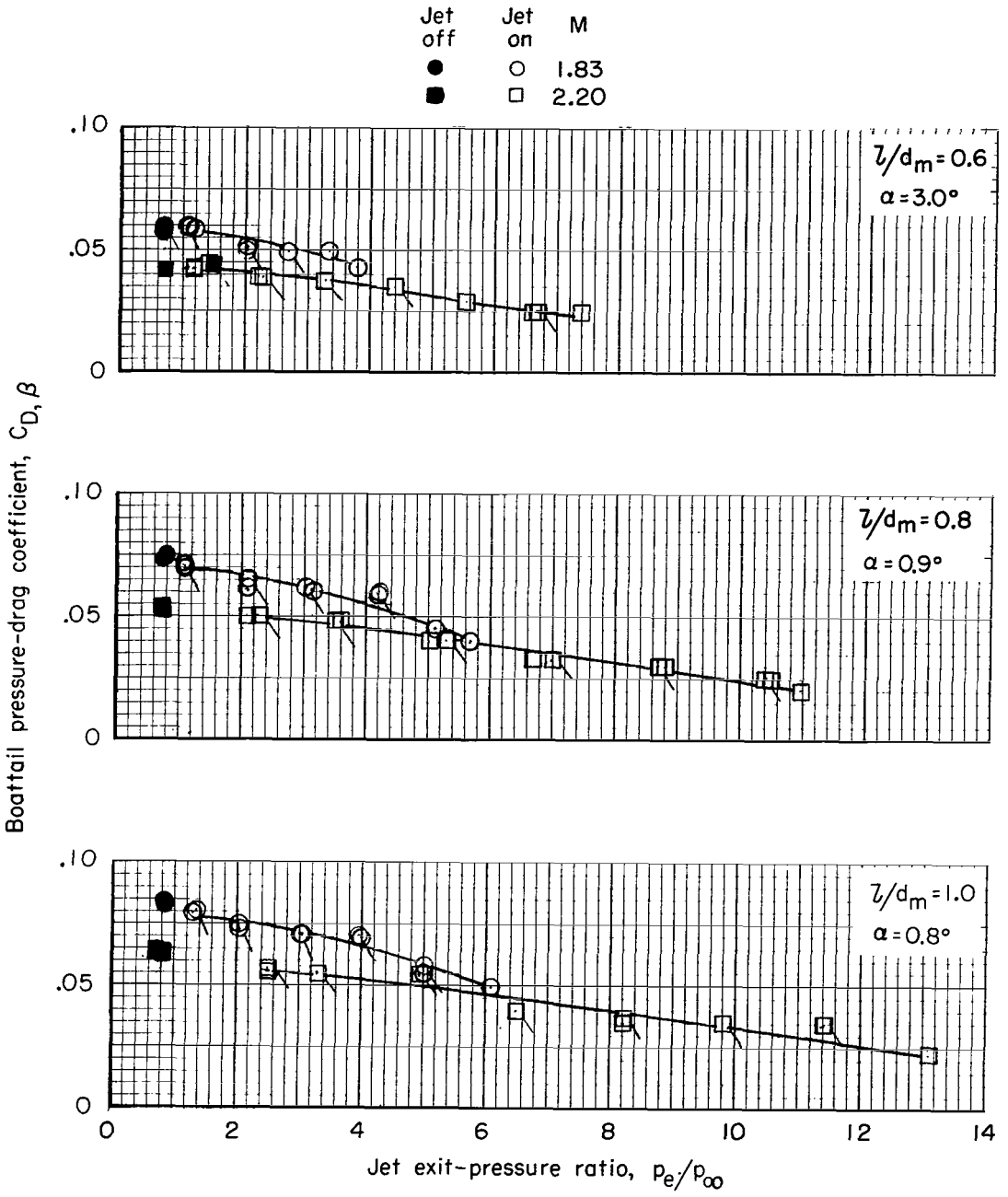

(c) $\beta = 10°$.

Figure 13.- Concluded.

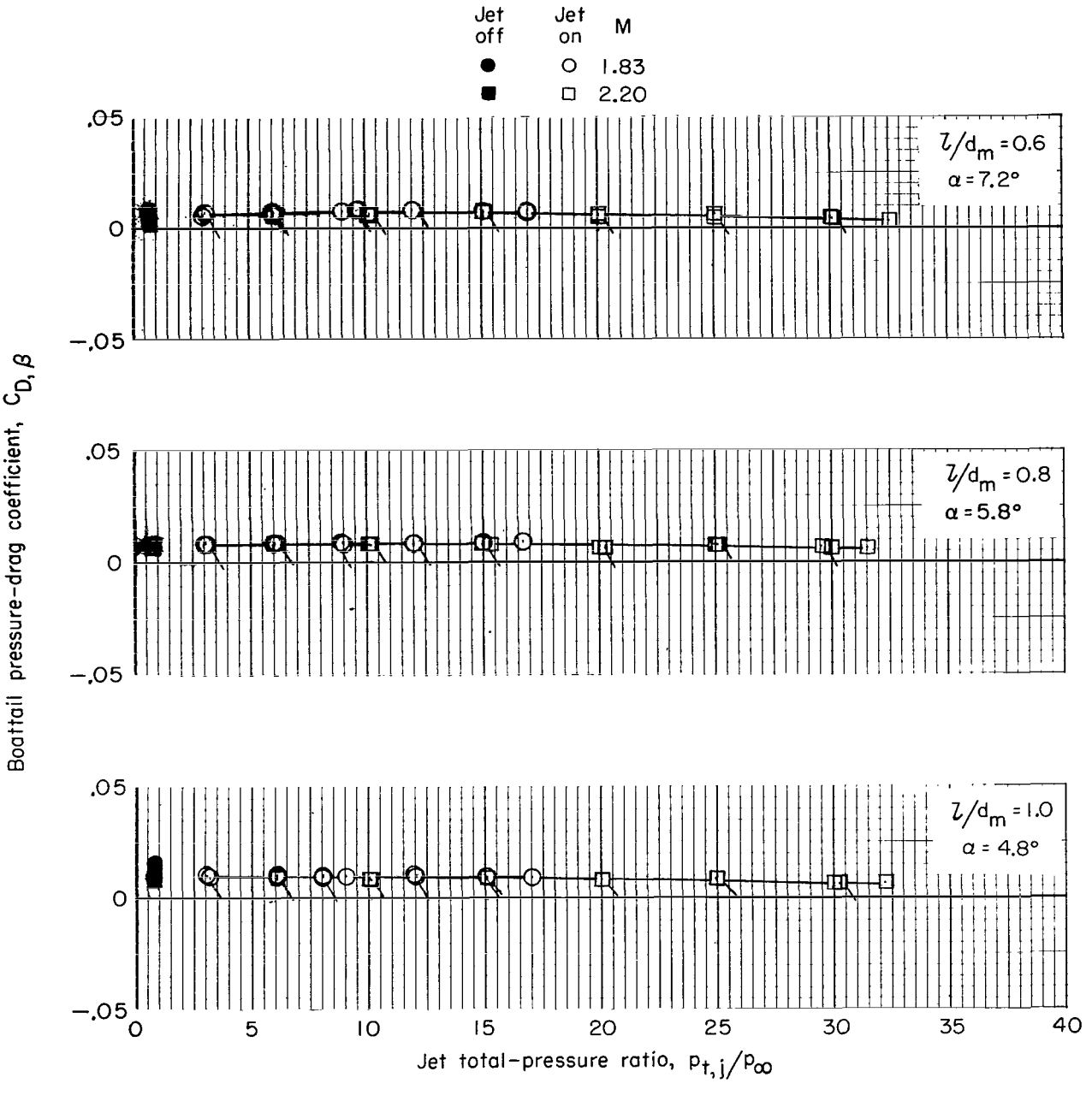

(a) $\beta \approx 3^o$.

Figure 14.- Variation of boattail pressure-drag coefficient with jet total-pressure ratio. Flagged symbols indicate data taken as pressure ratio was decreased.

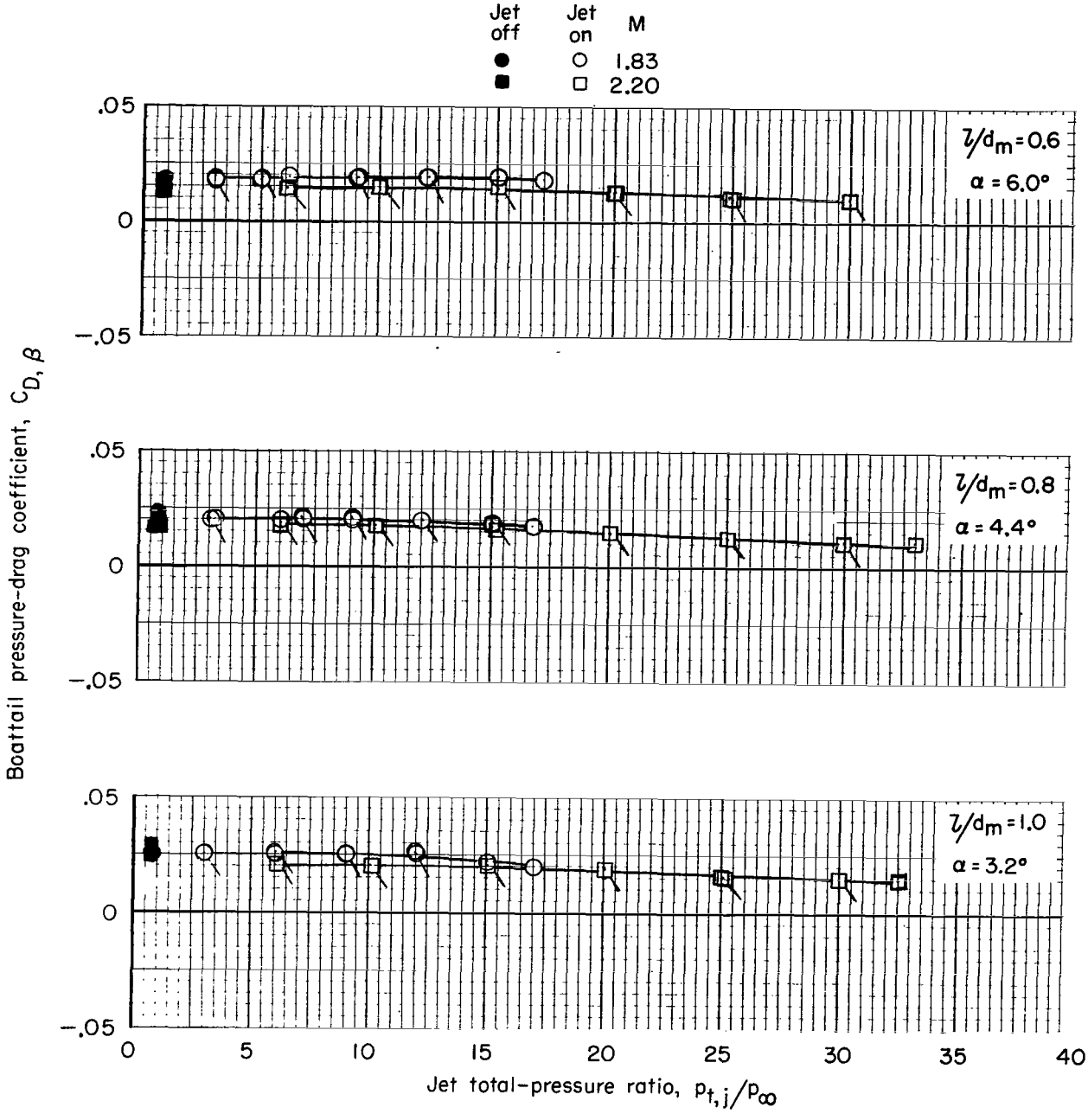

(b) $\beta = 5^{o}$.

Figure 14.- Continued.

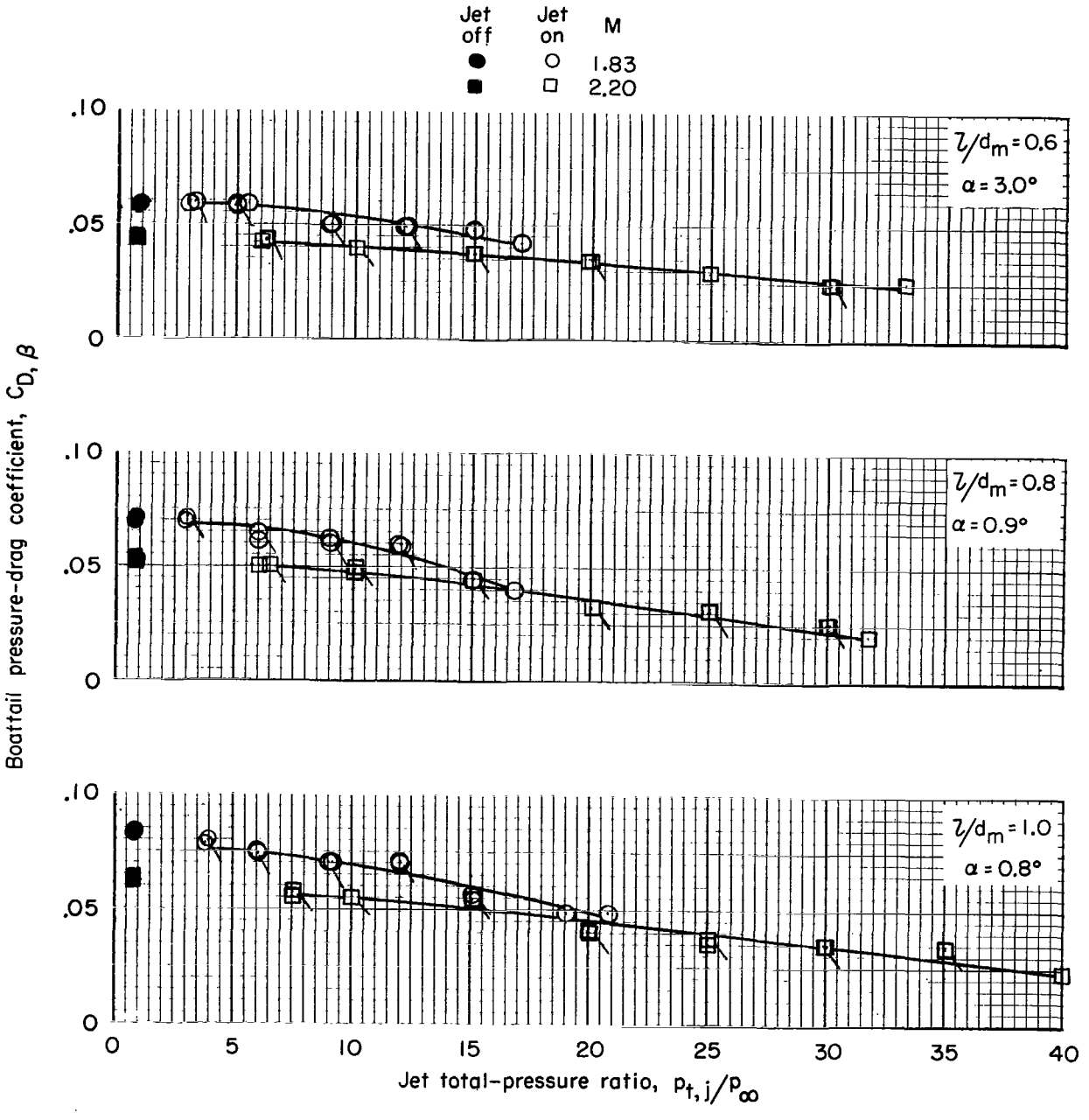

(c) $\beta = 10^o$.

Figure 14.- Concluded.

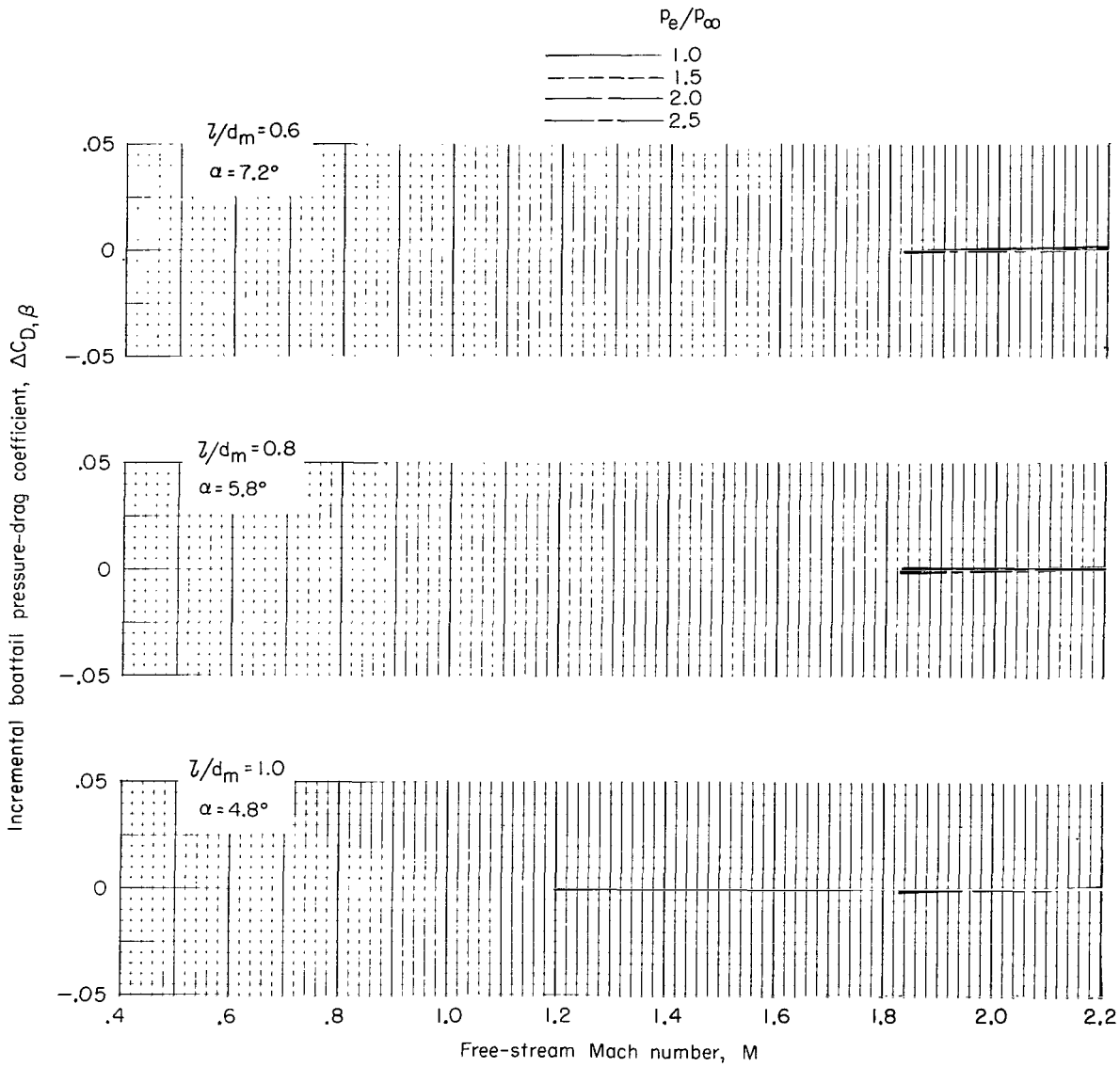

(a) $\beta \approx 3^o$.

Figure 15.- Effect of Mach number on incremental boattail pressure-drag coefficient due to jet operation. (Data at Mach numbers of 1.3 and lower are from ref. 1.)

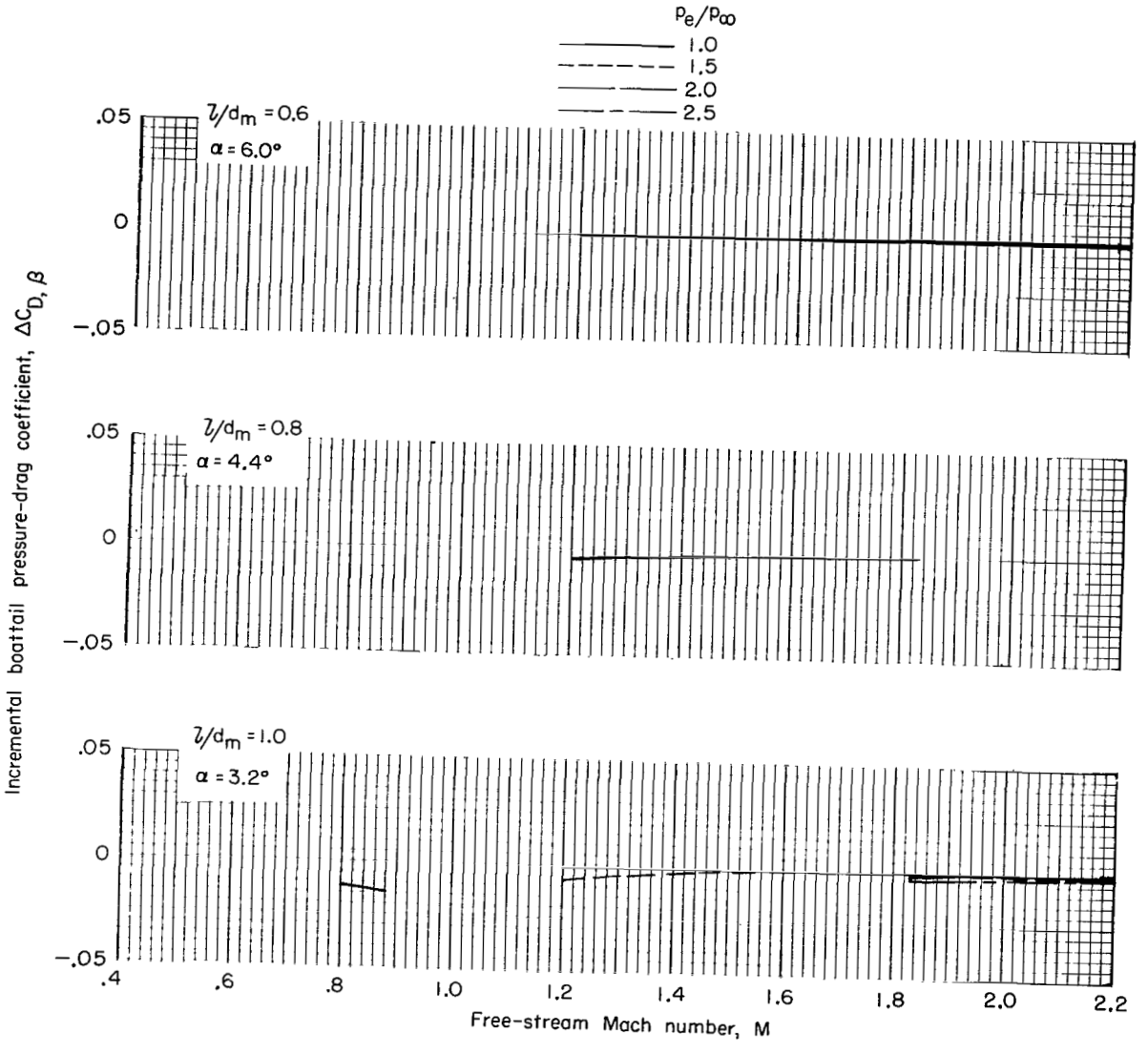

(b) $\beta = 5^o$.

Figure 15.- Continued.

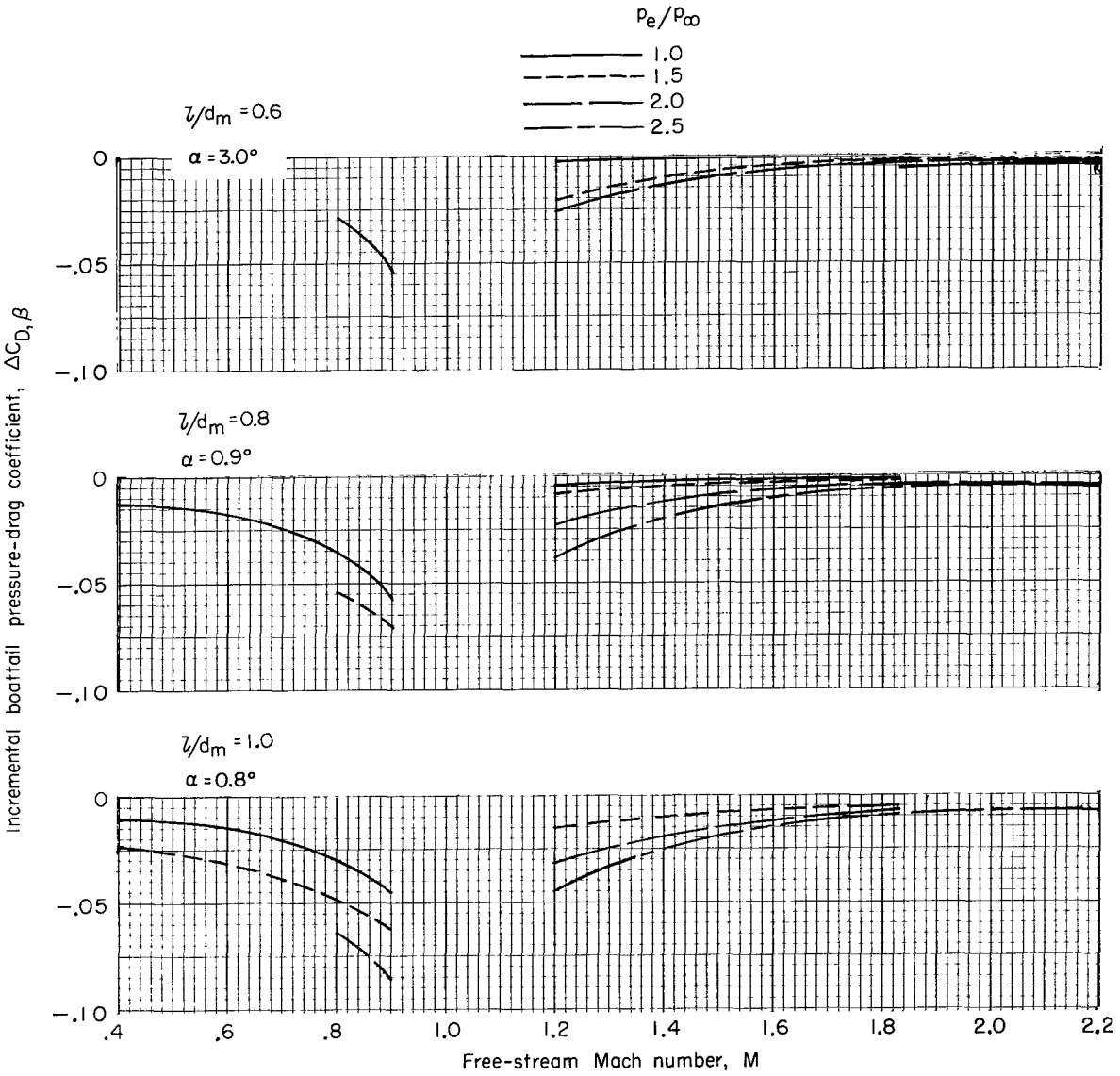

(c) $\beta = 10^o$.

Figure 15.- Concluded.

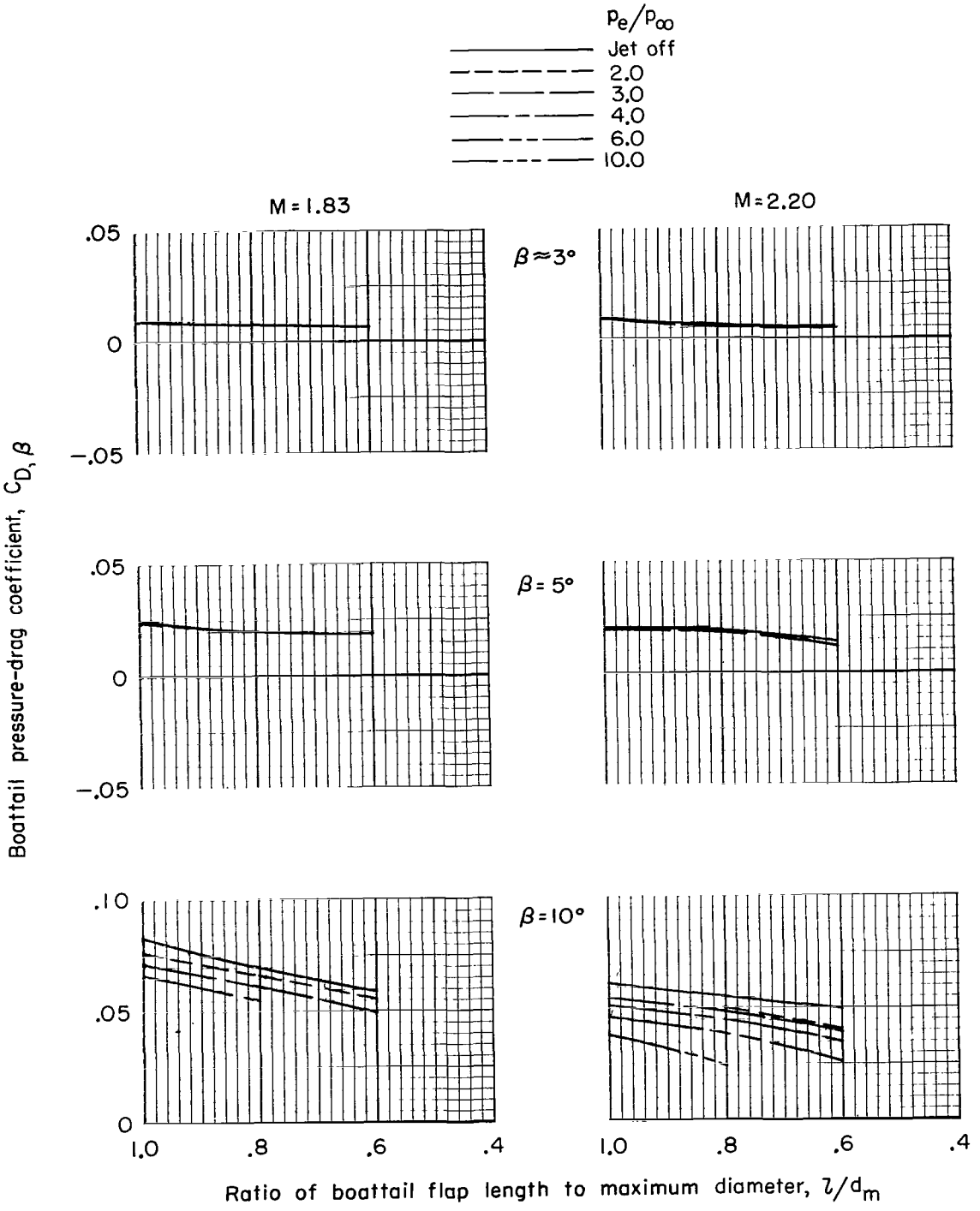

Figure 16.- Variation of boattail pressure-drag coefficient with the ratio of boattail flap length to maximum diameter for various jet-exit static-pressure ratios.

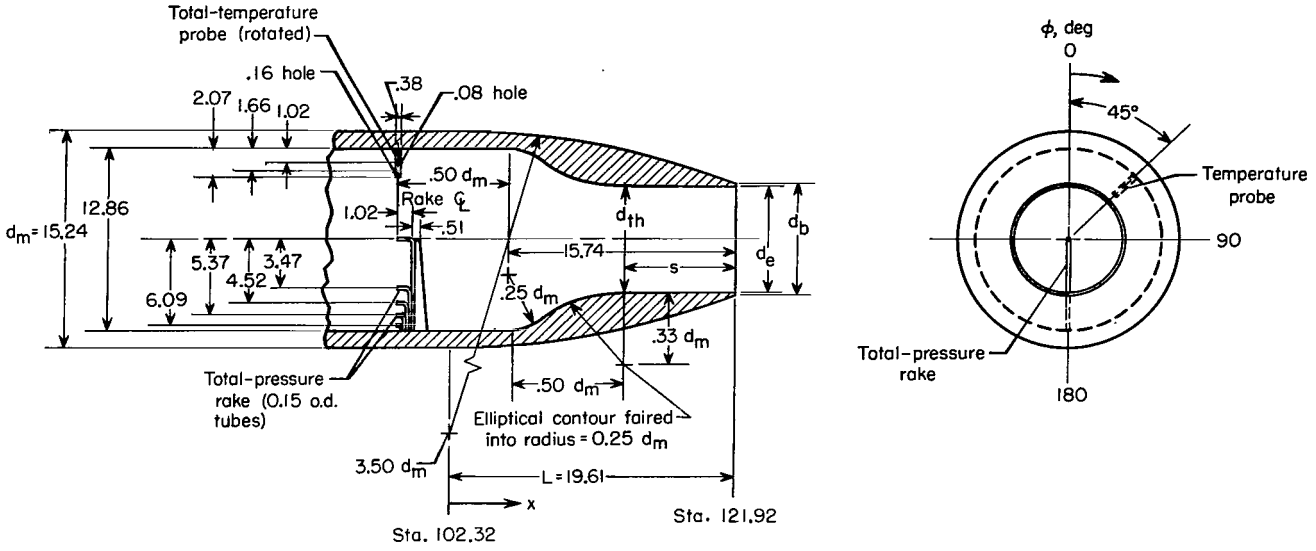

Static orifice locations					
External			Internal		
ϕ, deg	x/d_m [1]	x/L	ϕ, deg	Axial location	x/L
0	-0.17	-0.13	0, 90, and 270	In plane of rake	-0.19
	0	0			
	.19	.15			
	.38	.29			
	.56	.44			
	.75	.58			
	.93	.72			
	1.11	.86			
	1.19	.93	315	3.81 cm from exit	0.81
	1.27	.99			
90 and 180	0	0		0.22 cm from exit (base pressure)	0.99
	.19	.15			
	.38	.29			
	.56	.44			
	.75	.58			
	.93	.72			
	1.11	.86			
	1.19	.93			
	1.27	.99			

Dimensional and geometric parameters	
d_{th} = 7.62	d_b = 7.77
L/d_m = 1.286	d_b/d_m = 0.510
A_b/A_m = 0.260	A_e/A_b = 0.962
A_{th}/A_m = 0.250	s/d_{th} = 1.000
ϵ_e = 1.000	

Figure 17.- Sketch of S.T.A. nozzle showing geometry and orifice locations. Dimensions are in centimeters unless otherwise indicated.

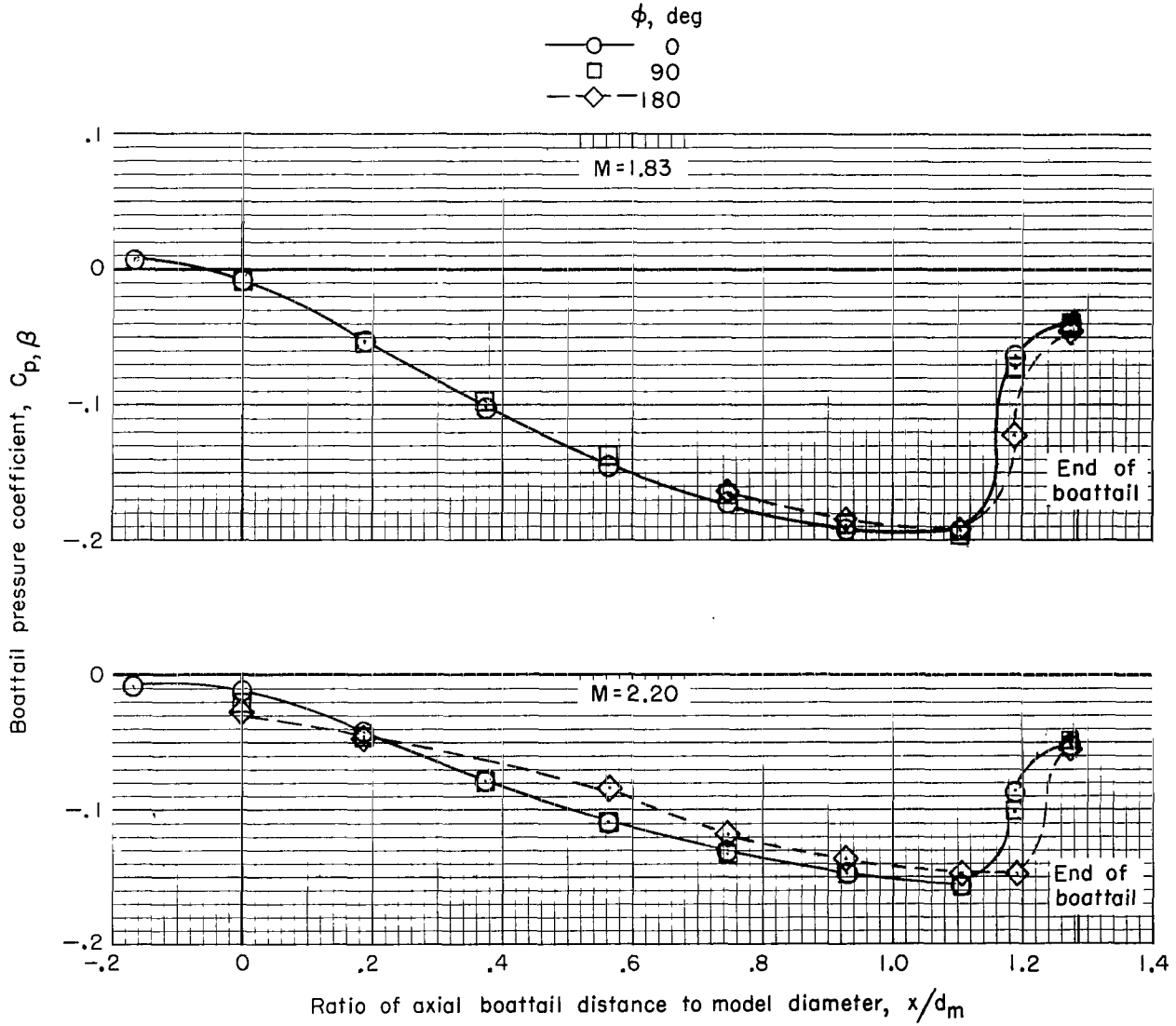

Figure 18.- Boattail pressure-coefficient distributions for several values of ϕ on reference nozzle. Jet off.

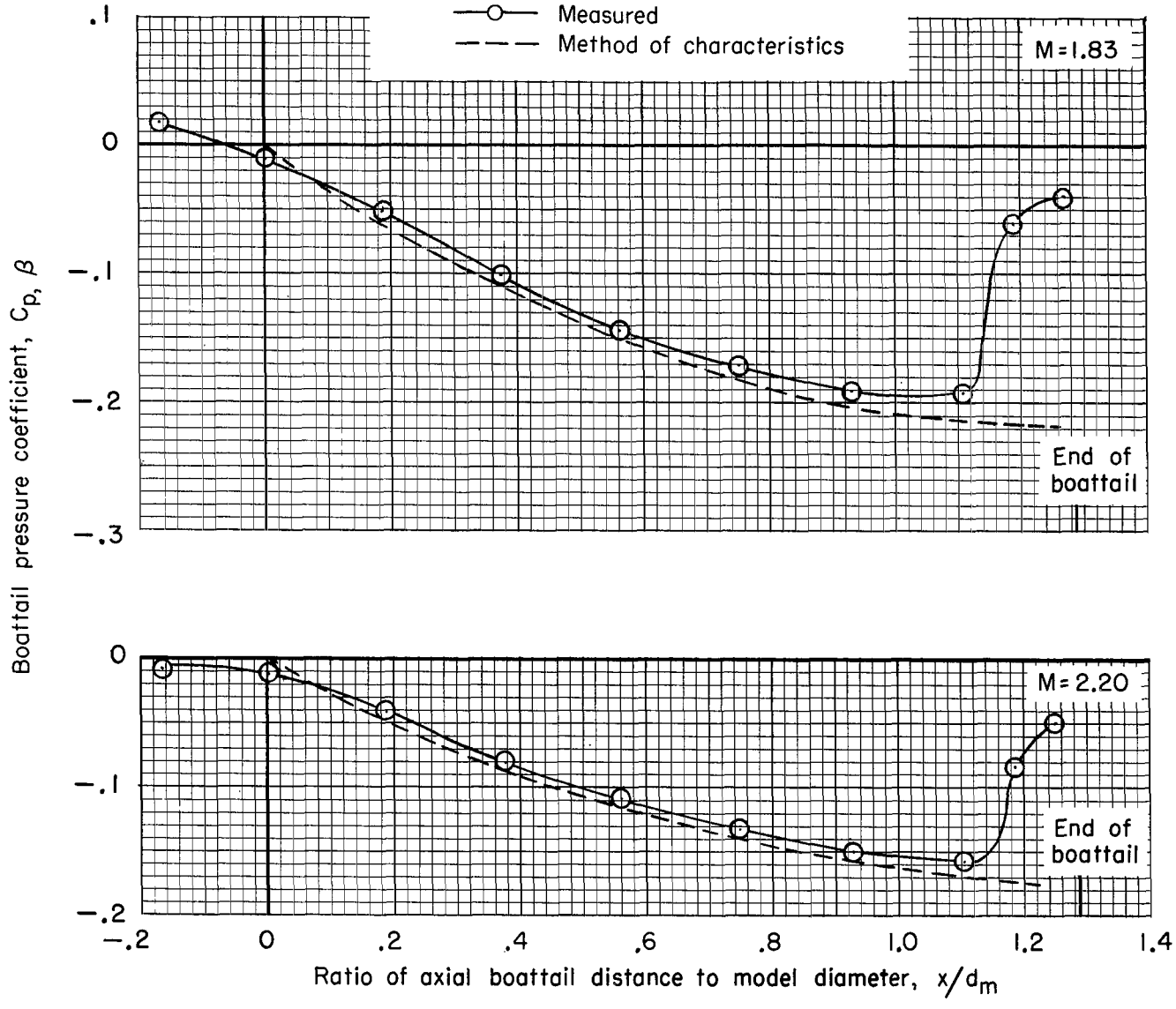

Figure 19.- Comparison of measured and theoretical boattail pressure-coefficient distributions for the reference nozzle. Jet off; $\phi = 0^o$.

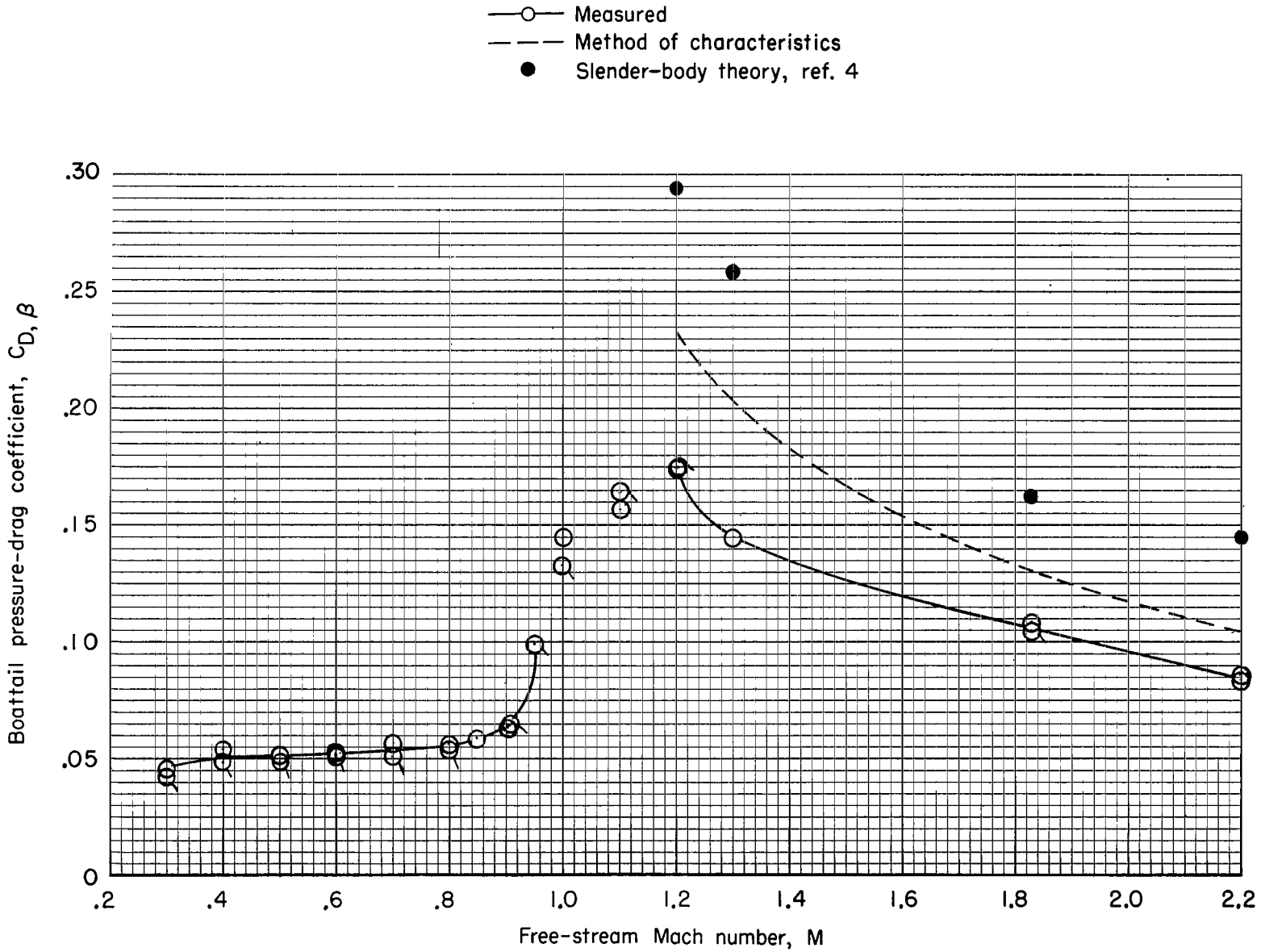

Figure 20.- Boattail pressure-drag coefficient as a function of Mach number for the reference nozzle. Jet off. Flagged symbols indicate repeat data.

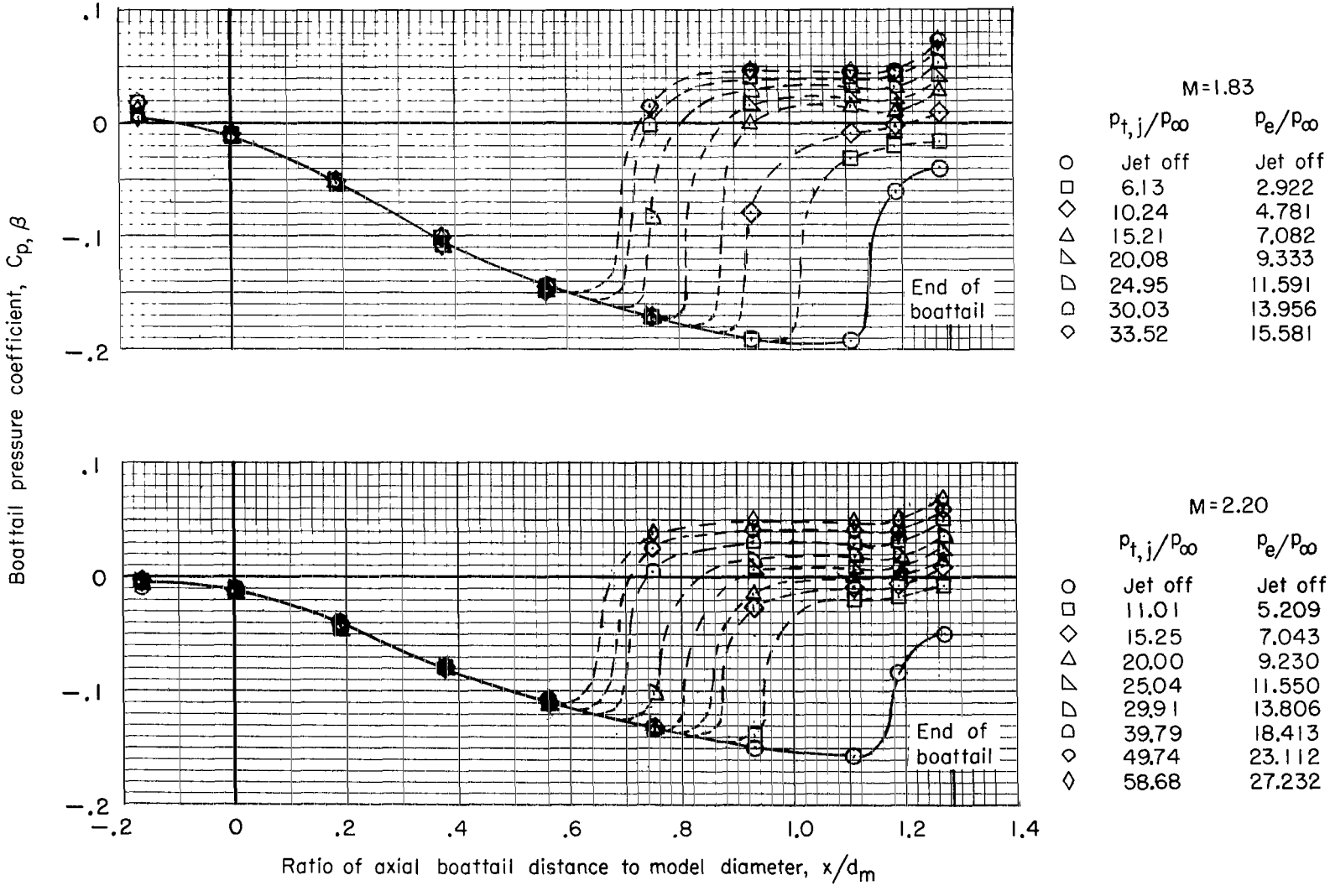

Figure 21.- Boattail pressure-coefficient distributions for reference nozzle at various jet pressure ratios. $\phi = 0^o$.

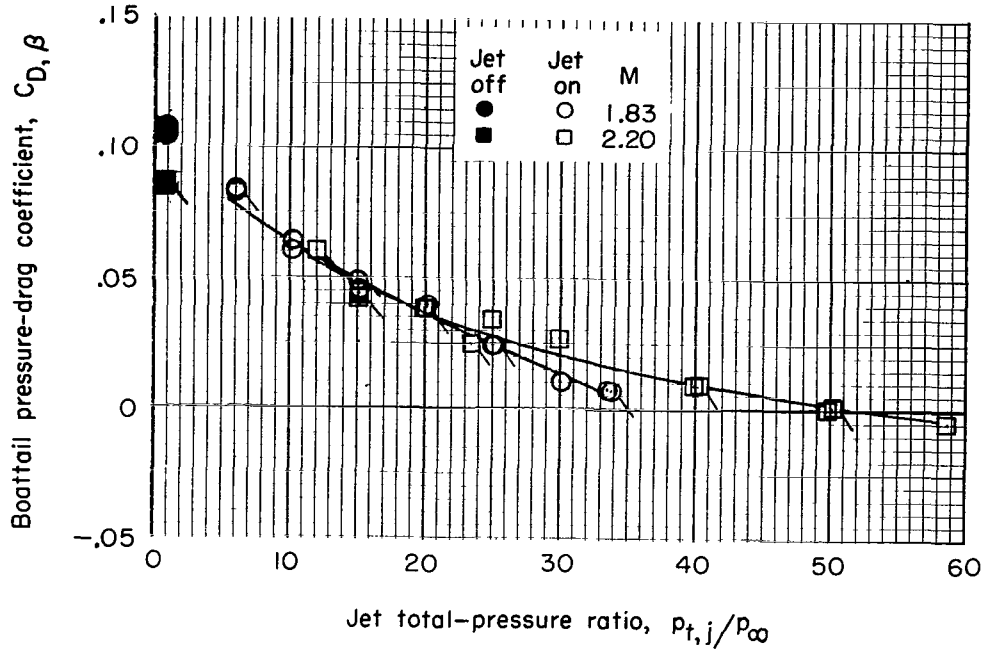

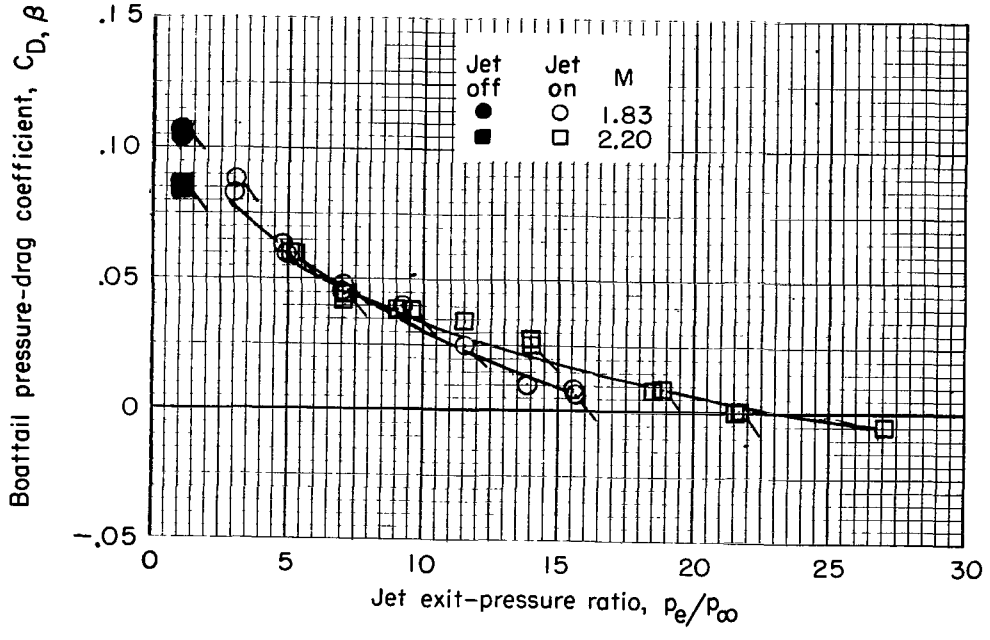

Figure 22.- Boattail pressure-drag coefficient as a function of jet pressure ratio for reference nozzle. Flagged symbols indicate data taken as pressure ratio was decreased.

NASA-Langley, 1972 —— 1 L-8139

"The aeronautical and space activities of the United States shall be conducted so as to contribute . . . to the expansion of human knowledge of phenomena in the atmosphere and space. The Administration shall provide for the widest practicable and appropriate dissemination of information concerning its activities and the results thereof."

—NATIONAL AERONAUTICS AND SPACE ACT OF 1958

NASA SCIENTIFIC AND TECHNICAL PUBLICATIONS

TECHNICAL REPORTS: Scientific and technical information considered important, complete, and a lasting contribution to existing knowledge.

TECHNICAL NOTES: Information less broad in scope but nevertheless of importance as a contribution to existing knowledge.

TECHNICAL MEMORANDUMS: Information receiving limited distribution because of preliminary data, security classification, or other reasons.

CONTRACTOR REPORTS: Scientific and technical information generated under a NASA contract or grant and considered an important contribution to existing knowledge.

TECHNICAL TRANSLATIONS: Information published in a foreign language considered to merit NASA distribution in English.

SPECIAL PUBLICATIONS: Information derived from or of value to NASA activities. Publications include conference proceedings, monographs, data compilations, handbooks, sourcebooks, and special bibliographies.

TECHNOLOGY UTILIZATION PUBLICATIONS: Information on technology used by NASA that may be of particular interest in commercial and other non-aerospace applications. Publications include Tech Briefs, Technology Utilization Reports and Technology Surveys.

Details on the availability of these publications may be obtained from:

SCIENTIFIC AND TECHNICAL INFORMATION OFFICE

NATIONAL AERONAUTICS AND SPACE ADMINISTRATION

Washington, D.C. 20546